



Effective field theory for nuclear vibrations with quantified uncertainties

E. A. Coello Pérez¹ and T. Papenbrock^{1,2}

¹*Department of Physics and Astronomy, University of Tennessee, Knoxville, Tennessee 37996, USA*

²*Physics Division, Oak Ridge National Laboratory, Oak Ridge, Tennessee 37831, USA*

(Received 9 October 2015; published 14 December 2015)

We develop an effective field theory (EFT) for nuclear vibrations. The key ingredients—quadrupole degrees of freedom, rotational invariance, and a breakdown scale around the three-phonon level—are taken from data. The EFT is developed for spectra and electromagnetic moments and transitions. We employ tools from Bayesian statistics for the quantification of theoretical uncertainties. The EFT consistently describes spectra and electromagnetic transitions for ^{62}Ni , $^{98,100}\text{Ru}$, $^{106,108}\text{Pd}$, $^{110,112,114}\text{Cd}$, and $^{118,120,122}\text{Te}$ within the theoretical uncertainties. This suggests that these nuclei can be viewed as anharmonic vibrators.

DOI: [10.1103/PhysRevC.92.064309](https://doi.org/10.1103/PhysRevC.92.064309)

PACS number(s): 21.60.Ev, 21.10.Ky, 21.10.Re, 27.60.+j

I. INTRODUCTION

The quest for quadrupole vibrations in atomic nuclei is a long and confusing one. Based on the groundbreaking work by Bohr and Mottelson [1–3], low-energy excitations of atomic nuclei are viewed as quadrupole oscillations of the liquid-drop surface. This approach suggests that some spherical nuclei can be viewed as harmonic quadrupole oscillators; i.e., the five-dimensional U(5) symmetric harmonic oscillator determines their spectra and low-lying transitions. Cadmium isotopes, for instance, have been employed as textbook cases of vibrational motion [3–5]. While corresponding harmonic spectra (including one-, two-, and possibly three-phonon states) were early identified in several nuclei, $B(E2)$ transition strengths exhibit considerable deviations from the predictions of the harmonic quadrupole oscillator; see, e.g., Refs. [6–17] for recent references to a long-standing problem [3,18]. Proposed anharmonicities were deemed insufficient to account for the considerable differences between data and the harmonic model [3,19]. Particularly concerning were the considerable variance between $B(E2)$ strengths for decays from two-phonon states (predicted to be equal) and the relatively large diagonal quadrupole matrix elements of low-lying 2^+ and 4^+ states (predicted to vanish); see, e.g., Refs. [20–22]. The observed deviations from the harmonic quadrupole oscillator are sometimes attributed to deformation of these thought-to-be-spherical nuclei.

Based on the data it is clear that harmonic quadrupole vibrations have not (yet) been observed in atomic nuclei. It is not clear, however, how to understand the vibrational spectra that are evident in many nuclei. In this paper, we reexamine nuclear vibrations within an effective field theory (EFT). The key ingredients of the EFT—quadrupole degrees of freedom, spherical symmetry, the separation of scales between low-lying collective excitations and a breakdown scale at about the three-phonon level—are consistent with data for spins and parities of low-lying states in the nuclei we wish to describe. The low-energy scale is approximately $\omega \approx 0.6$ MeV in nuclei of mass number 100, while the breakdown scale $\Lambda \approx 3\omega$ is attributable to pairing effects and other excluded physics. At leading order (LO), the EFT yields the harmonic quadrupole oscillator. The breakdown scale is based on the observed proliferation of states at about the three-phonon level, which

is clearly incompatible with the expectations from the LO Hamiltonian. In an EFT, corrections to the LO Hamiltonian are attributable to the excluded physics beyond the breakdown scale. A power counting can be used to estimate their size and to systematically improve the Hamiltonian—order by order—as well as transition operators. This is the program we follow in this paper.

We note that EFTs now have a decades-old history in the physics of nuclei. Most effort has been dedicated to an EFT of the interactions between nucleons itself; see Refs. [23–26] for reviews. Paired with *ab initio* calculations [27–29], such interactions now provide us with a model-independent approach to atomic nuclei. Halo EFT exploits the separation of scales between weakly bound halo nucleons and core excitations at much higher energy [30–33]. The EFT for heavy deformed nuclei [34,35] exploits the separation of scales between low-lying rotational modes and higher-energetic vibrations that result from the quantization of Nambu-Goldstone modes in finite systems [36,37].

In this paper we also spend a considerable effort on the quantification of theoretical uncertainties. If a theoretical result is within the experimental uncertainties, theorists usually claim success. However, for meaningful predictions, theoretical uncertainties are crucial. Likewise, disagreement between theoretical results and data can only be claimed based on the absence of overlap between theoretical and experimental uncertainties. Thus, the claim that traditional vibrational models do not describe the existing data is hard to quantify in the absence of theoretical uncertainties. This makes uncertainty quantification particularly relevant for this work.

When it comes to theoretical uncertainties, EFTs have a key advantage over models. The power counting immediately provides the EFT practitioner with uncertainty estimates. Very recently, progress has also been made toward the quantification of uncertainties [38–42] using Bayesian statistics. In an EFT, uncertainties can be quantified because the (testable) expectation of “naturalness” can be encoded into priors. Here one assumes that natural-sized coefficients govern the EFT expansion for observables. In this work, we build on these advances and also present analytical formulas for uncertainty quantification based on log-normal priors that are so relevant for EFTs.

This paper is organized as follows. In Sec. II, we develop the EFT for nuclear vibrations and construct the Hamiltonian and electromagnetic operators. In Sec. III we employ Bayesian tools for uncertainty quantification based on the assumption of natural sized coefficients in the EFT expansion for observables. We compare theoretical results with data for spectra and for electromagnetic moments and transitions in Secs. IV and V, respectively. Finally, we present our summary in Sec. VI. More detailed derivations are relegated to the Appendix.

II. EFFECTIVE THEORY FOR QUADRUPOLE VIBRATORS

In this section, we develop the EFT for nuclear vibrations. As our intended audience is wide, we aim at a self-contained description. In the following sections we introduce the LO Hamiltonian, discuss the power counting and higher-order corrections, and develop electromagnetic couplings and observables.

A. Leading-order Hamiltonian and spectrum

The spins and parities of low-energy spectra of even-even nuclei near shell closures suggest these can be described in terms of quadrupole degrees of freedom. In several cases, the spectrum resembles—at least at low energies—that of a quadrupole harmonic oscillator. In nuclei with mass number about 100, the oscillator spacing is $\omega \approx 0.6$ MeV. The fermionic nature of the nucleus manifests itself through pair-breaking effects, which enter at about 2–3 MeV of excitation [43]. Thus, the breakdown scale is $\Lambda \approx 3\omega$, and for definiteness we set $\Lambda = 3\omega$ in this work.

The boson creation and annihilation operators d_μ^\dagger and d_μ with $\mu = -2, -1, \dots, 2$, respectively, fulfill the usual commutation relations

$$[d_\mu^\dagger, d_\nu] = -\delta_\mu^\nu. \quad (1)$$

We note that d_μ^\dagger are the components of the rank 2 spherical tensor d^\dagger . For the general construction of spherical tensors we also introduce the spherical rank 2 tensor \tilde{d} with components

$$\tilde{d}_\mu = (-1)^\mu d_{-\mu}. \quad (2)$$

For the construction of spherical tensors we follow Ref. [44] and introduce tensor products and scalar products. The spherical tensor $\mathcal{I}^{(I)}$ of rank I ,

$$\mathcal{I}^{(I)} = (\mathcal{M}^{(I_1)} \otimes \mathcal{N}^{(I_2)})^{(I)}, \quad (3)$$

results from coupling the spherical tensors $\mathcal{M}^{(I_1)}$ and $\mathcal{N}^{(I_2)}$ of ranks I_1 and I_2 , respectively. Its components,

$$\mathcal{I}_M^{(I)} = \sum_{M_1 M_2} C_{I_1 M_1 I_2 M_2}^{I M} \mathcal{M}_{M_1}^{(I_1)} \mathcal{N}_{M_2}^{(I_2)}, \quad (4)$$

are given in terms of the Clebsch-Gordan coefficients $C_{I_1 M_1 I_2 M_2}^{I M}$ that couple spins I_1 and I_2 to spin I . Similarly, the scalar product of two spherical tensors $\mathcal{M}^{(I)}$ and $\mathcal{N}^{(I)}$ of the same

rank I is

$$\mathcal{M}^{(I)} \cdot \mathcal{N}^{(I)} = \sum_{\mu} (-1)^\mu \mathcal{M}_{\mu}^{(I)} \mathcal{N}_{-\mu}^{(I)} \quad (5)$$

$$= \sqrt{2I+1} (\mathcal{M}^{(I)} \otimes \mathcal{N}^{(I)})^{(0)}. \quad (6)$$

There are two simple operators we need to consider. The number operator

$$\hat{N} \equiv d^\dagger \cdot \tilde{d} \quad (7)$$

is a scalar that counts the total number of phonons N . The angular momentum operator is the vector

$$\hat{\mathbf{I}} = \sqrt{10} (d^\dagger \otimes \tilde{d})^{(1)}. \quad (8)$$

Both operators conserve the number of phonons. We note that the commutation relations

$$[\hat{I}_\mu, d_\nu^\dagger] = \sqrt{6} C_{2\nu 1\mu}^{2\nu+\mu} d_{\nu+\mu}^\dagger, \quad (9)$$

$$[\hat{I}_\mu, \tilde{d}_\nu] = \sqrt{6} C_{2\nu 1\mu}^{2\nu+\mu} \tilde{d}_{\nu+\mu}, \quad (10)$$

clearly identify d^\dagger and \tilde{d} as spherical tensors of rank 2. In contrast, d_μ are not components of a spherical tensor.

The Hamiltonian must be a scalar under rotation. The simplest (i.e., quadratic in the fields d^\dagger and \tilde{d}) Hamiltonian is

$$\begin{aligned} \hat{H}_{\text{LO}} &= \omega \hat{N} \\ &= \omega \sum_{\mu} (-1)^\mu d_\mu^\dagger \tilde{d}_{-\mu} \\ &= \omega \sum_{\mu} d_\mu^\dagger d_\mu. \end{aligned} \quad (11)$$

Here ω is a low-energy constant (LEC) that has to be adjusted to data. We note that one could also consider an operator proportional to

$$d^\dagger \cdot d^\dagger + \tilde{d} \cdot \tilde{d} \quad (12)$$

as part of the LO Hamiltonian. However, a Bogoliubov transformation that introduces (quasi-)boson creation and annihilation operators

$$D_\mu^\dagger = u_\mu^* d_\mu^\dagger + v_\mu^* \tilde{d}_\mu, \quad D_\mu = u_\mu d_\mu + v_\mu \tilde{d}_\mu^\dagger, \quad (13)$$

with $|u_\mu|^2 - |v_\mu|^2 = 1$, would transform such a Hamiltonian into the diagonal form

$$\hat{H}_{\text{LO}} = \tilde{\omega} (D^\dagger \cdot \tilde{D}). \quad (14)$$

Here \tilde{D} is defined in terms of D similar to Eq. (2). This Hamiltonian conserves the number of (quasi-)bosons and cannot be distinguished from the LO Hamiltonian (11).

Clearly, the LO Hamiltonian of the EFT for nuclear vibrations is equivalent to the quadrupole vibrator submodel of the Bohr Hamiltonian [1–3,5,45]. We note that the five-dimensional quadrupole oscillator exhibits an U(5) symmetry. Within the EFT approach, this symmetry is a (trivial) consequence of the choice of degrees of freedom and the quadratic LO Hamiltonian. While this symmetry might be useful in labeling basis states, it does not reflect symmetry properties of the interaction between nucleons.

The energies of the LO Hamiltonian

$$\hat{H}_{\text{LO}} |\psi\rangle = E_{\text{LO}} |\psi\rangle \quad (15)$$

are

$$E_{LO} = \omega N. \quad (16)$$

For the construction of the eigenstates we follow Rowe and Wood and also refer the reader to Ref. [46]. The eigenstates of the LO Hamiltonian can be labeled by the quantum numbers of the symmetry subgroups in the chain

$$\begin{array}{ccccccc} U(5) & \supset & SO(5) & \supset & U(3) & \supset & SO(3) & \supset & SO(2) \\ N & & \nu & & \nu & & I & & M \end{array}.$$

Here ν is a radial quantum number, I and M are the usual $SO(3)$ angular momentum and its projection onto the z axis, while the seniority ν is the $SO(5)$ analog of the angular momentum. From now on, we refer to the $SO(3)$ angular momentum as spin.

The ground state of the system is the phonon vacuum, denoted by $|0\rangle$. A state with N excited quanta is created from the vacuum by the application of N creation operators, coupled to appropriate spin. Given the quantum numbers ν and ν , the highest-weight state is defined by

$$|N = \nu + 2\nu, \nu, \nu, I = 2\nu, M = 2\nu\rangle \propto (d^\dagger \cdot d^\dagger)^\nu (d_2^\dagger)^\nu |0\rangle. \quad (17)$$

Here the proportionality sign expresses the absence of proper normalization on the right-hand side. The remaining states with $N = \nu + 2\nu$ phonons can be reached from the highest-weight states by the application of suitably defined lowering operators. This construction is similar to the construction of $SO(3)$ irreducible eigenstates where one starts from the state $|I, M = I\rangle$ and obtains the remaining states of the spin- I multiplet by successive application of the spin-lowering operator. For the LO Hamiltonian, one finds a singlet with spin $I = 2$ at the one-phonon level, a triplet with spins $I = 0, 2, 4$ at the two-phonon level, and a quintuplet with spins $I = 0, 2, 3, 4, 6$ at the three-phonon level. It is convenient to determine the LEC ω from the excitation energy of the one-phonon state.

B. Power counting and next-to-leading-order corrections

Quadrupole excitations are the low-lying collective degrees of freedom in even-even nuclei near shell closures. This picture breaks down at higher energies Λ where the microscopic structure of the nucleus in terms of underlying fermionic nucleons is resolved.

In an EFT, subleading corrections to the Hamiltonian arise owing to the omitted degrees of freedom. As one can write an unlimited number of rotational scalars in the fields d^\dagger and \tilde{d} , we need a power counting (in powers of the small parameter ω/Λ) for the systematic construction of the EFT. As the fields d^\dagger and \tilde{d} do not carry any dimension, we introduce quadrupole coordinates $\tilde{\alpha}$ and momenta π as

$$\tilde{\alpha}_\mu \equiv \sqrt{\frac{1}{2}} \ell (d_\mu^\dagger + \tilde{d}_\mu), \quad (18)$$

$$\pi_\mu = i \sqrt{\frac{1}{2}} \ell^{-1} (d_\mu^\dagger - \tilde{d}_\mu). \quad (19)$$

Here $\ell \equiv (B\omega)^{-1/2}$ is the oscillator length, and B is a mass parameter. These degrees of freedom fulfill the canonical

commutation relations

$$[\pi_\mu, \alpha_\nu] = -i \delta_{\mu\nu}, \quad \tilde{\alpha}_\mu = (-1)^\mu \alpha_{-\mu}. \quad (20)$$

We note that both $\tilde{\alpha}$ and π are spherical tensors of rank 2. In terms of them, the LO Hamiltonian can be written as

$$\hat{H}_{LO} = \frac{1}{2B} (\pi \cdot \pi + B^2 \omega^2 \tilde{\alpha} \cdot \tilde{\alpha}) - \frac{5}{2} \omega. \quad (21)$$

Thus, the sizes of coordinates and momenta at the N -phonon level are

$$\tilde{\alpha} \sim \sqrt{N} \ell \quad \text{and} \quad \pi \sim \sqrt{N} \ell^{-1}. \quad (22)$$

At the breakdown scale, we have, by definition,

$$B\omega^2 \tilde{\alpha}^2 \sim \Lambda \quad \text{and} \quad \frac{\pi^2}{B} \sim \Lambda. \quad (23)$$

Thus,

$$\tilde{\alpha} \sim \sqrt{\frac{\Lambda}{\omega}} \ell \quad \text{and} \quad \pi \sim \sqrt{\frac{\Lambda}{\omega}} \ell^{-1} \quad (24)$$

at the breakdown scale.

Let us write the subleading corrections to the Hamiltonian (11) as rotationally invariant terms of the form $g_{mn} \pi^m \tilde{\alpha}^n$, with $m+n > 2$. At the breakdown scale Λ , the energy shift owing to these corrections must be so large that N -phonon states cannot be distinguished from states with $N \pm 1$ phonons. Thus,

$$g_{mn} \pi^m \tilde{\alpha}^n \sim \omega, \quad (25)$$

and this implies

$$g_{mn} \sim \ell^{m-n} \left(\frac{\omega}{\Lambda} \right)^{\frac{m+n}{2}} \omega \quad (26)$$

for the natural size of these coefficients. When the term $g_{mn} \pi^m \tilde{\alpha}^n$ is evaluated for coordinates and momenta of size (22), it scales as

$$g_{mn} \pi^m \tilde{\alpha}^n \sim \varepsilon^{\frac{m+n}{2}} \omega. \quad (27)$$

Here

$$\varepsilon \equiv (N\omega/\Lambda) \quad (28)$$

is the relevant dimensionless expansion parameter of our EFT at the N -phonon level. We note that LO energies scale as $\varepsilon^0 \omega$.

This simple analysis suggests that terms cubic in the quadrupole fields are the dominant subleading corrections. However, such terms change boson number and thus enter only in second-order perturbation theory, yielding a contribution of size $\varepsilon^3 \omega$. Thus, the next-to-leading-order (NLO) contributions come from those terms quartic in the quadrupole fields that preserve the boson number. They contribute corrections of the size $\varepsilon^2 \omega$. We note that some collective models differ from the EFT's power counting by employing cubic terms as dominant subleading corrections; see, e.g., Refs. [19,47–50]. We also note that the proliferation of higher-order terms was addressed in some models by only considering certain combinations of operators that are symmetric under exchange of the operators.

We can now also consider the power counting directly for the operators d^\dagger and \tilde{d} . When acting on states at the breakdown scale, $d^\dagger \sim \tilde{d} \sim \sqrt{\Lambda/\omega}$. Demanding that a Hamiltonian term

of the form $\omega f_m d^m$ containing m boson operators is of size ω at the breakdown scale thus yields $f_m \sim (\omega/\Lambda)^{m/2}$, and the whole term $\omega f_m d^m$ scales as $\sim \omega(\omega/\Lambda)^{m/2}$ at low energies.

Before we continue, it is interesting to discuss an alternative—and less conservative—understanding of the breakdown scale. One could also assume that the energy corrections of the terms $g_{mn}\pi^m\tilde{\alpha}^n$ (for $m+n > 2$) are of size Λ (and not ω) at the breakdown scale. Then the contributions from such terms scale as $g_{mn}\pi^m\tilde{\alpha}^n \sim (\omega/\Lambda)^{(m+n)/2}\Lambda$ at low energies. This implies that the off-diagonal terms with $m+n=3$ contribute an energy $\sim \omega^2/\Lambda$ in second-order perturbation theory, and this is equal to the contribution of the $m+n=4$ terms in first-order perturbation theory. Such an approach would again differ from the early approach [19] because terms with four boson operators are as important as terms with three boson operators. Compared to the more conservative approach we are taking, this would add two additional terms [namely, $(\pi \times \pi)^{(2)} \cdot \tilde{\alpha}$ and $(\tilde{\alpha} \times \tilde{\alpha})^{(2)} \cdot \tilde{\alpha}$] at NLO, increasing the number of unknown LECs considerably. Such an approach would also probably increase the breakdown scale beyond the three-phonon level, making it difficult to identify states at higher energies. Therefore, we did choose a more conservative—and physically better motivated—power counting.

To identify the linearly independent NLO terms that conserve phonon number, we turned to Chap. 3 of Ref. [44] and determined the following three terms:

$$\hat{N}^2 = (d^\dagger \cdot \tilde{d})^2, \quad (29)$$

$$\hat{\Lambda}^2 = -(d^\dagger \cdot d^\dagger)(\tilde{d} \cdot \tilde{d}) + \hat{N}^2 - 3\hat{N}, \quad (30)$$

$$\hat{I}^2 = 10(d^\dagger \otimes \tilde{d})^{(1)} \cdot (d^\dagger \otimes \tilde{d})^{(1)}. \quad (31)$$

Here the operator $\hat{\Lambda}$ is the SO(5) analog of the spin \hat{I} (see, e.g., Ref. [5]). The action of these operators on the LO states is

$$\hat{N}^2|N\nu\nu IM\rangle = N^2|N\nu\nu IM\rangle, \quad (32)$$

$$\hat{\Lambda}^2|N\nu\nu IM\rangle = \nu(\nu+3)|N\nu\nu IM\rangle, \quad (33)$$

$$\hat{I}^2|N\nu\nu IM\rangle = I(I+1)|N\nu\nu IM\rangle. \quad (34)$$

Thus, at NLO the Hamiltonian takes the form $\hat{H}_{\text{NLO}} = \hat{H}_{\text{LO}} + \hat{h}_{\text{NLO}}$, with

$$\hat{h}_{\text{NLO}} = g_N \hat{N}^2 + g_\nu \hat{\Lambda}^2 + g_I \hat{I}^2. \quad (35)$$

Here the LECs g_N , g_ν , and g_I have to be adjusted to data. The action of the NLO correction (35) on the eigenstates of the LO Hamiltonian yields

$$\hat{h}_{\text{NLO}}|N\nu\nu IM\rangle = e_{\text{NLO}}|N\nu\nu IM\rangle, \quad (36)$$

with

$$e_{\text{NLO}} = g_N N^2 + g_\nu \nu(\nu+3) + g_I I(I+1). \quad (37)$$

The total energy at NLO is thus

$$E_{\text{NLO}} = E_{\text{LO}} + e_{\text{NLO}}. \quad (38)$$

The four LECs ω , g_N , g_ν , and g_I can be determined from the energies of the one-phonon state and the two-phonon states. Higher excited states would then be predictions. It is clear that the quest for higher precision of the EFT, e.g.,

by including next-to-next-to-leading-order terms introduces further LECs and requires even more data to determine the Hamiltonian. This loss of predictive power is unsatisfactory, but it is also clear that an approach solely based on symmetry arguments—as proposed in this work—naturally leads to this state of affairs. We note that the previous approaches [47–50] avoid the proliferation of new coupling constants by only considering certain combinations of higher-order terms. From the EFT's perspective, however, such a selection does not constitute a systematic approach.

The breakdown scale $\Lambda \approx 3\omega$ is not sufficiently large to study contributions beyond NLO. To improve predictive capabilities, we quantify (rather than estimate) theoretical uncertainties. This is done in Sec. III.

C. Electromagnetic couplings

Our EFT deals with quadrupole degrees of freedom. As the gauge potential $\mathbf{A}(\mathbf{r})$ is a vector field, the electromagnetic coupling of the EFT is not obvious. We can view the quadrupole degrees of freedom as components of a scalar field that depends on the position coordinate \mathbf{r} . This view suggests to employ $\mathbf{r} = r\mathbf{e}_r(\theta, \phi)$ (with \mathbf{e}_r being the usual radial unit vector [44]) and to expand the vector potential as [51]

$$\mathbf{A}(r, \Omega) = \sum_{JM} \sum_l A_{JM,l} j_l(kr) \sum_{mn} C_{lm1n}^{JM} Y_{lm}(\Omega) \mathbf{e}_n.$$

Here we employed spherical basis vectors \mathbf{e}_n with $n = -1, 0, 1$, and j_l denotes the spherical Bessel function. The spherical wave has a momentum k . We note that $A_{JM,l}$ are components of a tensor of rank J for fixed l .

The quadrupole degrees of freedom of the EFT must couple to the components $A_{2M,l}$, and only $l = 1, 2, 3$ contribute owing to triangular relations on spins. In the long wavelength approximation $kr \ll 1$, and $j_l(kr) \propto (kr)^l$. Thus, $A_{2M,1}$ is the dominant contribution, and we gauge

$$\pi_\mu \rightarrow \pi_\mu - q A_{2\mu,1}. \quad (39)$$

Here the charge q is a LEC that needs to be adjusted to data. We are interested in single-photon transitions and only consider terms linear in \mathbf{A} . The effective electric quadrupole operator, resulting from gauging the LO Hamiltonian (11), is thus

$$\begin{aligned} \hat{Q}_{\text{LO}} &= -\frac{q}{B} \sum_{\mu} (-1)^{\mu} A_{2-\mu,1} \pi_{\mu} \\ &= -\frac{iq}{\sqrt{2}B\ell} \sum_{\mu} (-1)^{\mu} A_{2-\mu,1} (d_{\mu}^{\dagger} - \tilde{d}_{\mu}). \end{aligned} \quad (40)$$

Let us also consider higher-order corrections. Hamiltonian terms involving two momentum operators π_{μ} and one coordinate operator $\tilde{\alpha}_{\mu}$ contribute to the energy at next-to-next-to-leading order and were beyond the NLO corrections discussed in this section. When considering single-photon transitions, gauging essentially replaces one of the two momentum operators by the gauge field and couples the latter to an operator of the structure

$$(\pi \times \tilde{\alpha})^{(2)} \propto -i(d^{\dagger} \times d^{\dagger} - \tilde{d} \times \tilde{d})^{(2)}. \quad (41)$$

The EFT expectation is that this operator yields a correction of relative size $\varepsilon^{1/2}$ to the LO operator (40). It induces transitions between states that differ by two phonon numbers, and we come back to this point after discussing nonminimal couplings.

Let us also consider nonminimal couplings and work in the Coulomb gauge. Then, the electric field is $\mathbf{E} = -\partial_t \mathbf{A} = -ik\mathbf{A}$. Here we assumed an exponential time dependence and set the speed of light to $c = 1$. We note that $k \approx \omega$ for transitions between states that differ by one phonon number. The electric field has an expansion similar to Eq. (39), and the expansion coefficients fulfill $E_{JM,l} = -ikA_{JM,l}$. The electric field couples to the quadrupole operator

$$\hat{Q}_\mu = \frac{\sqrt{2}}{\ell} Q_0 \tilde{\alpha}_\mu + \frac{2}{\ell^2} Q_1 (\tilde{\alpha} \times \tilde{\alpha})_\mu^{(2)} + \frac{2\sqrt{2}}{\ell^3} \sum_{L=0,2,4} Q_{2L} [\tilde{\alpha} \times (\tilde{\alpha} \times \tilde{\alpha})]_\mu^{(2L)} + \dots \quad (42)$$

Here factors of the oscillator length ℓ have been inserted such that the LECs Q_0 , Q_1 , and Q_{2L} have the dimension of a quadrupole moment. The factors of $\sqrt{2}$ are inserted for convenience. The expansion of the quadrupole moment should not be a surprise: What is not forbidden by symmetries is allowed in an EFT. We recall that truly “elementary” degrees of freedom couple to electromagnetic gauge fields solely via minimal coupling. The EFT, however, does not deal with elementary degrees of freedom. The quadrupole coordinates of the EFT are effective degrees of freedom at low energies. They are composite and describe collective effects of more microscopic “high-energy” degrees of freedom that are not resolved at the low-energy scale we are interested in. The nonminimal couplings allow us to incorporate the subleading electromagnetic effects of any microscopic degrees of freedom. Based on the EFT power counting, the natural sizes of the LECs Q_1 and Q_{2L} are

$$Q_1 \sim \left(\frac{\omega}{\Lambda}\right)^{1/2} Q_0, \quad Q_{2L} \sim \frac{\omega}{\Lambda} Q_0. \quad (43)$$

It is useful to rewrite the expansion (42) in terms of creation and annihilation operators. This yields

$$\begin{aligned} \hat{Q}_\mu &= Q_0 (d_\mu^\dagger + \tilde{d}_\mu) + Q_1 (d^\dagger \times d^\dagger + \tilde{d} \times \tilde{d} + 2d^\dagger \times \tilde{d})_\mu^{(2)} \\ &+ \sum_{L=0,2,4} Q_{2L} [d^\dagger \times (d^\dagger \times d^\dagger)^{(L)} + \tilde{d} \times (\tilde{d} \times \tilde{d})^{(L)} \\ &+ d^\dagger \times (d^\dagger \times \tilde{d})^{(L)} + d^\dagger \times (\tilde{d} \times \tilde{d})^{(L)} + \dots]_\mu^{(2)} \\ &+ \dots \end{aligned} \quad (44)$$

Let us consider the right-hand side of Eq. (44). The first line is the LO term for transitions between states that differ by one phonon number. It is equivalent to the term (40) obtained from gauging. This allows us to identify

$$q = \sqrt{2} B k \ell Q_0. \quad (45)$$

The second line of Eq. (44) is the LO term for transitions between states that differ by none or two phonon numbers

and also determines diagonal quadrupole matrix elements. Thus, diagonal quadrupole matrix elements are expected to be a factor $\sqrt{\omega/\Lambda}$ smaller than transition quadrupole moments between states that differ by one phonon number. The expected finite value for diagonal quadrupole matrix elements is a significant departure from vanishing diagonal quadrupole matrix elements obtained for the harmonic quadrupole vibrator. The third line has NLO corrections (LO terms) for quadrupole transitions between states that differ by one (three) phonon numbers. Thus, the expectations from the harmonic quadrupole vibrator that $B(E2)$ transitions from the two-phonon states to the one-phonon state are independent of the initial spin are expected to suffer corrections of relative size ω/Λ . We note that all anharmonic corrections vanish in the harmonic limit, i.e., for $\omega/\Lambda \rightarrow 0$.

The reduced matrix elements of a tensor operator \hat{O} of rank λ between two states $|i\rangle$ and $|f\rangle$ are defined as

$$\langle f || \hat{O} || i \rangle = \frac{\sqrt{2I_f + 1}}{C_{I_f M_f, I_i M_i, \lambda \mu}} \langle \beta I_f M_f | \hat{O}_\mu | \alpha I_i M_i \rangle. \quad (46)$$

Here β and α denote quantum numbers irrelevant for the reduced matrix elements. For transitions between states differing by one phonon number we find the well-known LO reduced matrix elements

$$\begin{aligned} \langle 0_1^+ || \hat{Q} || 2_1^+ \rangle_{\text{LO}} &= Q_0 \langle 0_1^+ || d || 2_1^+ \rangle = \sqrt{5} Q_0, \\ \langle 2_1^+ || \hat{Q} || 0_2^+ \rangle_{\text{LO}} &= Q_0 \langle 2_1^+ || d || 0_2^+ \rangle = \sqrt{2} Q_0, \\ \langle 2_1^+ || \hat{Q} || 2_2^+ \rangle_{\text{LO}} &= Q_0 \langle 2_1^+ || d || 2_2^+ \rangle = \sqrt{10} Q_0, \\ \langle 2_1^+ || \hat{Q} || 4_1^+ \rangle_{\text{LO}} &= Q_0 \langle 2_1^+ || d || 4_1^+ \rangle = \sqrt{18} Q_0, \end{aligned} \quad (47)$$

and uncertainty estimates are of order $Q_0 \omega/\Lambda$.

For transitions between two-phonon states we find

$$\begin{aligned} \langle 2_2^+ || \hat{Q} || 0_2^+ \rangle_{\text{LO}} &= 2Q_1 \langle 2_2^+ || (d^\dagger \times \tilde{d})^{(2)} || 0_2^+ \rangle \\ &= 4Q_1, \\ \langle 2_2^+ || \hat{Q} || 4_1^+ \rangle_{\text{LO}} &= 2Q_1 \langle 2_2^+ || (d^\dagger \times \tilde{d})^{(2)} || 4_1^+ \rangle \\ &= \frac{24}{7} Q_1, \end{aligned} \quad (48)$$

and uncertainty estimates are of order $Q_1 \omega/\Lambda$.

For the diagonal quadrupole matrix elements we find the LO reduced matrix elements

$$\begin{aligned} \langle 2_1^+ || \hat{Q} || 2_1^+ \rangle_{\text{LO}} &= 2Q_1 \langle 2_1^+ || (d^\dagger \times \tilde{d})^{(2)} || 2_1^+ \rangle \\ &= 2\sqrt{5} Q_1, \\ \langle 2_2^+ || \hat{Q} || 2_2^+ \rangle_{\text{LO}} &= 2Q_1 \langle 2_2^+ || (d^\dagger \times \tilde{d})^{(2)} || 2_2^+ \rangle \\ &= -\frac{6\sqrt{5}}{7} Q_1, \\ \langle 4_1^+ || \hat{Q} || 4_1^+ \rangle_{\text{LO}} &= 2Q_1 \langle 4_1^+ || (d^\dagger \times \tilde{d})^{(2)} || 4_1^+ \rangle \\ &= \frac{6\sqrt{110}}{7} Q_1, \end{aligned} \quad (49)$$

and uncertainty estimates are of order $Q_1 \omega/\Lambda$. Thus, the LEC Q_1 relates the three diagonal matrix elements (49) and the two

transition matrix elements (48) to each other. This prediction of the EFT is tested in Sec. V.

For the transition involving a change by two phonons we find

$$\begin{aligned} \langle 0_1^+ || \hat{Q} || 2_2^+ \rangle_{\text{LO}} &= Q_1 \langle 0_1^+ || (\tilde{d} \times \tilde{d})^{(2)} || 2_2^+ \rangle \\ &= \sqrt{10} Q_1, \end{aligned} \quad (50)$$

and uncertainty estimates are of order $Q_1 \omega / \Lambda$. This nonminimal correction is of the same size as the NLO correction (41) from gauging. The combination of both terms involves the LEC of the term from gauging and the LEC Q_1 . As there is only one $E2$ transition in vibrational nuclei below the breakdown energy (i.e., the three-phonon energy), the EFT has no predictive power for this transition beyond an estimate of its natural size. Therefore, we do not consider it here.

The $B(E2)$ transition strengths are given in terms of the reduced matrix elements as

$$B(E2, I_i \rightarrow I_f) = \frac{|\langle I_f || Q || I_i \rangle|^2}{2I_i + 1}. \quad (51)$$

We finally also turn to magnetic moments. In the EFT at LO, magnetic moments are attributable to the vector operator

$$\hat{\mu} = g \hat{I}, \quad (52)$$

and g is a LEC constant. Thus, magnetic moments of states with spin I have the reduced matrix elements

$$\langle I || \hat{\mu} || I \rangle = g \sqrt{I(I+1)(2I+1)}. \quad (53)$$

Corrections from omitted higher-order terms are of relative size $\varepsilon^{1/2}$ [e.g., from terms such as $(\tilde{\alpha} \times \hat{\mu})^{(1)}$]. At LO, magnetic moments of $I = 4$ states are a factor $\sqrt{6}$ larger than magnetic moments of $I = 2$ states. This is another testable prediction of the EFT.

It is interesting to note that anharmonic corrections to the quadrupole operator have been considered early on [3,19]. However, Bès and Dussel related the expansion coefficients of the quadrupole operator to those of the Hamiltonian (also using terms cubic in the boson annihilation and creation operators as corrections to the harmonic quadrupole vibrator). While such an approach has fewer adjustable parameters than the EFT we constructed, it did not yield a satisfactory description of ^{114}Cd . Of course, there are no symmetry arguments that would link the expansion coefficients of nonminimal couplings and the Hamiltonian.

Let us briefly recall the adjustable parameters. The EFT for nuclear vibrations employs one LEC at LO [namely, ω in Eq. (16)] and three additional LECs at NLO [namely, g_N , g_v , and g_I in Eq. (37)] for the Hamiltonian. These LECs need to be adjusted to the energies of four states below the three-phonon level. Thus, LO has predictive power, while NLO has predictive power only for states at the three-phonon level. As we see in Sec. IV, NLO predictions for the energy of the 6_1^+ state are more accurate than expected.

Below the three-phonon level there are four strong $E2$ transitions ($2_1^+ \rightarrow 0_1^+$, $0_2^+ \rightarrow 2_1^+$, $2_2^+ \rightarrow 2_1^+$, $4_1^+ \rightarrow 2_1^+$) that change phonon number by one unit. They require the LEC Q_0 to be adjusted to data. The somewhat smaller matrix

elements that govern the two $E2$ transitions between the two-phonon states ($4_1^+ \rightarrow 2_2^+$, $2_2^+ \rightarrow 0_2^+$), and the three diagonal $E2$ matrix elements of the states 2_1^+ , 2_2^+ , and 4_1^+ require the LEC Q_1 to be adjusted to data. Finally, one LEC [namely g in Eq. (53)] determines the three magnetic moments of the 2_1^+ , 2_2^+ , and 4_1^+ states. In this way, the EFT provides us with model-independent relations between observables.

III. QUANTIFIED THEORETICAL UNCERTAINTIES

The quantification of theoretical uncertainties is of growing interest in nuclear physics. For a wide collection of articles on this topic we refer the reader to the 2015 focus issue and its editorial [52].

The power counting provides the EFT practitioner with a simple tool to *estimate* theoretical uncertainties as missing contributions from higher orders. In our case, uncertainties at LO are of the size $\mathcal{O}(\varepsilon^2 \omega)$ (as they are caused by missing NLO contributions), while uncertainties at NLO are of the size $\mathcal{O}(\varepsilon^3 \omega)$ (owing to contributions beyond NLO). In such estimates, one implicitly assumes that the dimensionless coefficients in front of these order-of-magnitude estimates are of order one.

To *quantify* (rather than estimate) theoretical uncertainties requires considerable effort [41,53]. In this section, we follow Refs. [39,40,42] and employ Bayesian statistics for uncertainty quantification. Within this approach, theoretical uncertainties can be expressed as degree-of-belief (DOB) intervals and have a statistical meaning. The construction of such DOB intervals requires one to make detailed quantitative assumptions about the behavior of omitted orders in the power counting. As a result, theoretical predictions and uncertainties can be confronted by data (and underlying assumptions can be verified, or modified if required).

A. Analytical results for log-normal priors

In this section we follow Furnstahl *et al.* and present the formalism required for uncertainty quantification. We also present a few analytical expressions that involve log-normal priors, which are particularly useful when “naturalness” arguments are employed in EFTs.

We are interested in uncertainty estimates for observables computed in an EFT. The power counting, i.e., a small ratio $\varepsilon < 1$ [cf. Eq. (28)] of the low-energy scale and the breakdown scale, allows us to expand an observable X as

$$X = X_0 \sum_{n=0}^{\infty} c_n \varepsilon^n. \quad (54)$$

Here X_0 sets the general scale. In practice, the sum above can only be computed up to and including the term involving ε^k . This implies that the relative uncertainty is

$$\Delta_k = \sum_{n=k+1}^{\infty} c_n \varepsilon^n. \quad (55)$$

It is our aim to quantify the uncertainty Δ_k . We are particularly interested in quantifying the residual,

$$\Delta_k^{(M)} = \sum_{n=k+1}^{k+M} c_n \varepsilon^n, \quad (56)$$

of the first M missing terms. To quantify uncertainties, one has to make quantitative assumptions about the distribution of the expansion coefficients c_n . A key assumption is that the expansion coefficients are independent of each other, and assumptions about the distribution of expansion coefficients are employed as priors.

In an EFT, the expansion coefficients are assumed to be of order unity. The log-normal distribution

$$\text{pr}(c) = \frac{1}{\sqrt{2\pi}\sigma c} e^{-\frac{1}{2}\left(\frac{\log c}{\sigma}\right)^2} \quad (57)$$

is consistent with this assumption. Choosing, for instance, $\sigma = \log \alpha$ (with $\alpha > 1$) implies that $1/\alpha \leq c \leq \alpha$ with about 68% probability.

The expansion coefficient c_n is related to the prior (57) by a second prior $\text{pr}(c_n|c)$. We consider two examples. First, we assume that the log-normal distributed c yields a hard bound on the size of c_n . Thus,

$$\text{pr}^{(\text{hw})}(c_n|c) = \frac{1}{2c} \Theta(c - |c_n|). \quad (58)$$

Here $\Theta(x)$ denotes the unit step function. The priors (57) and (58) are ‘‘set B’’ of Ref. [42]. Alternatively, we assume that the log-normal distributed c is related to the width of the Gaussian prior,

$$\text{pr}^{(\text{G})}(c_n|c) = \frac{1}{\sqrt{2\pi}c} e^{-\frac{c_n^2}{2c^2}}. \quad (59)$$

Following [42] the application of Bayes’ theorem yields a probability distribution function for the uncertainty Δ , which we write as

$$p_M(\Delta|c_0, \dots, c_k) = \frac{\int_0^\infty dc \text{pr}(c) p_M(\Delta|c) \prod_{m=0}^k \text{pr}(c_m|c)}{\int_0^\infty dc \text{pr}(c) \prod_{m=0}^k \text{pr}(c_m|c)}. \quad (60)$$

Here the prior $\text{pr}(c)$ is the known (or expected) pdf and $\text{pr}(c_n|c)$ is the pdf for a specific expansion coefficient c_n given c . The probability of finding an uncertainty Δ given the prior for c is

$$p_M(\Delta|c) \equiv \left[\prod_{n=k+1}^{k+M} \int_{-\infty}^{\infty} dc_n \text{pr}(c_n|c) \right] \delta(\Delta - \Delta_k^{(M)}). \quad (61)$$

We note that the structure of Eq. (60) is quite intuitive. The numerator captures our understanding of how the uncertainty depends on the expansion coefficients given the pdf $\text{pr}(c)$, while the denominator is a normalization.

Reference [42] presents detailed discussions of $p_M(\Delta|c_0, \dots, c_k)$ for several combinations of priors but does not give analytical expressions for the log-normal distributed prior relevant for EFTs. In what follows, we derive analytical results for the pdf (60) based on the hard-wall prior (58) for $M = 1, 2$. For the Gaussian prior (59), we reduce the pdf (60) to single integrations for general M . We hope that

these formulas might be useful also for other applications of Bayesian uncertainty quantification in EFTs.

To make progress in computing the pdf (61), we rewrite the δ function as a Fourier integral

$$\delta(\Delta - \Delta_k^{(M)}) = \frac{1}{2\pi} \int_{-\infty}^{\infty} dt e^{it\Delta} \prod_{n=k+1}^{k+M} e^{-itc_n \varepsilon^n}.$$

Thus, $p_M(\Delta|c)$ is the Fourier transform of a product of Fourier transforms,

$$p_M(\Delta|c) = \frac{1}{2\pi} \int_{-\infty}^{\infty} dt e^{it\Delta} \prod_{n=k+1}^{k+M} \int_{-\infty}^{\infty} dc_n \text{pr}(c_n|c) e^{-it\varepsilon^n c_n}. \quad (62)$$

We evaluate the pdf (62) for the Gaussian prior (59) and find

$$p_M^{(\text{G})}(\Delta|c) = \frac{1}{\sqrt{2\pi}qc} e^{-\frac{\Delta^2}{2q^2c^2}}. \quad (63)$$

Here

$$q^2 \equiv \sum_{n=k+1}^{k+M} \varepsilon^{2n} = \varepsilon^{2k+2} \frac{1 - \varepsilon^{2M}}{1 - \varepsilon^2} \quad (64)$$

depends on M . Putting them all together, we are left with a single integration and can write

$$p_M^{(\text{G})}(\Delta|c_0, \dots, c_k) = \frac{1}{\sqrt{2\pi}q} \frac{\int_0^\infty dx x^{k+1} e^{-\frac{1}{2\sigma^2}[\log(x)]^2} e^{-\frac{\gamma^2 + \Delta^2/q^2}{2} x^2}}{\int_0^\infty dx x^k e^{-\frac{1}{2\sigma^2}[\log(x)]^2} e^{-\frac{\gamma^2}{2} x^2}}. \quad (65)$$

In this formula, the information from the expansion coefficients enters via

$$\gamma^2 \equiv \sum_{n=0}^k c_n^2. \quad (66)$$

The numerical evaluation of the pdf (65) poses no difficulty for any value of M . Formula (65) is one of the main results in this section.

Let us turn to the hard-wall prior (58). For the computation of the Fourier transform of the prior $\text{pr}^{(\text{hw})}(c_n|c)$ we use

$$\int_{-\infty}^{\infty} dc_n \text{pr}^{(\text{hw})}(c_n|c) e^{-itc_n \varepsilon^n} = \frac{\sin(c\varepsilon^n t)}{c\varepsilon^n t}, \quad (67)$$

and obtain the pdf for the uncertainty Δ as

$$p_M^{(\text{hw})}(\Delta|c) = \frac{1}{2\pi} \int_{-\infty}^{\infty} dt \cos(t\Delta) \prod_{n=k+1}^{k+M} \frac{\sin(c\varepsilon^n t)}{c\varepsilon^n t}. \quad (68)$$

As we will see, the integration over dt can be performed but becomes cumbersome for $M > 1$. Here we focus on $M = 1$ and present the result for $M = 2$ in the Appendix. For $M > 2$ it might be attractive to perform the integrations numerically. In this case, two integrations [one over dt for $p_M(\Delta|c)$ and one over dc] remain for the computation of Eq. (60), and this number is independent of M .

We set $M = 1$ in Eq. (68) and obtain [54]

$$p_1^{(\text{hw})}(\Delta|c) = \frac{1}{2c\varepsilon^{k+1}} \Theta(c\varepsilon^{k+1} - |\Delta|). \quad (69)$$

This result can also be written as $p_1^{(\text{hw})}(\Delta|c) = \text{pr}^{(\text{hw})}(\Delta|c\varepsilon^{k+1})$. It could also have been obtained by direct evaluation of the dc_{k+1} integration in Eq. (60) exploiting the δ function.

Let us compute $p_1^{(\text{hw})}(\Delta|c_0, \dots, c_k)$. We insert the pdf (69) and the priors (57) and (58) into Eq. (60) and perform the integrations (see the Appendix for details). This yields

$$p_1^{(\text{hw})}(\Delta|c_0, \dots, c_k) = \frac{e^{\frac{2k+3}{2}\sigma^2} 1 - \Phi\left(\frac{\sigma}{\sqrt{2}}\left(k+2 + \frac{\log b}{\sigma^2}\right)\right)}{2\varepsilon^{k+1} 1 - \Phi\left(\frac{\sigma}{\sqrt{2}}\left(k+1 + \frac{\log a}{\sigma^2}\right)\right)}, \quad (70)$$

Here $\Phi(x) \equiv (2/\sqrt{\pi}) \int_0^x dt \exp(-t^2)$ denotes the error function,

$$a \equiv \max(|c_0|, \dots, |c_k|), \quad (71)$$

and

$$b \equiv \max\left(a, \frac{|\Delta|}{\varepsilon^{k+1}}\right). \quad (72)$$

Let us discuss the result (70). Increasing Δ from zero, $p_1^{(\text{hw})}(\Delta|c_0, \dots, c_k)$ remains a constant for $b \leq a$, i.e., for $\Delta \leq a\varepsilon^{k+1}$. Past this point, $p_1^{(\text{hw})}(\Delta|c_0, \dots, c_k)$ decays rapidly to zero as $1 - \Phi$ approaches zero for increasing values of its argument.

For $x \gg 1$, we have

$$1 - \Phi(x) \approx \frac{e^{-x^2}}{\sqrt{\pi}x} \quad (73)$$

and obtain for $b \leq a$

$$p_1^{(\text{hw})}(\Delta|c_0, \dots, c_k) \approx \frac{1}{2a\varepsilon^{k+1}}. \quad (74)$$

Interestingly, the same value is found if the priors (57) and (58) are replaced by “set A” of Ref. [42]. This sheds light on the recent observation [42] that DOB percentages depend very mildly on the prior as k increases.

So far, we have limited our considerations to priors $\text{pr}(c_n|c)$ that have zero mean $\bar{c}_n = 0$. If one drives an EFT to sufficiently high order, one could actually study the distribution of the expansion coefficients c_n and thereby assess the prior. As we see below, priors of interest to our applications have a nonzero mean $\bar{c}_n \equiv \langle c_n \rangle \neq 0$. Thus, we need to include this information.

In what follows, we assume that the priors for c_n with $n \leq k$ have a nonzero mean \bar{c}_n , but keep the priors for c_{k+1}, c_{k+2}, \dots , with a zero mean (owing to lack of better knowledge). Then

$$p_M(\Delta|c_0, \dots, c_k) \rightarrow p_M(\Delta|c_0 - \bar{c}_0, \dots, c_k - \bar{c}_k); \quad (75)$$

i.e., one only subtracts the mean from the coefficients c_n with $n \leq k$ before inserting them into the analytical formulas.

For the Gaussian prior (59) we would also consider the modification that the log-normal distributed c is proportional (but not equal to) the width of the Gaussian. Thus, we introduce

a scale factor s and consider the prior

$$\text{pr}^{(\text{G})}(c_n|c) = \frac{1}{\sqrt{2\pi}sc} e^{-\left(\frac{c_n}{2sc}\right)^2}. \quad (76)$$

In this case, we need to replace $q \rightarrow sq$ in Eqs. (63) and (65).

Given an interval $[a, b]$ in the domain of a pdf $p(x)$, its DOB is defined as

$$\text{DOB}(a, b) = \int_a^b dx p(x). \quad (77)$$

We note that $\text{DOB}(a, b) \leq 1$, and the DOB of an interval represents the probability for the variable x to take a value within the interval $[a, b]$.

Our probability distributions $p_M(\Delta|c_0, \dots, c_k)$ are symmetric around $\Delta = 0$. We define the corresponding DOB as

$$\text{DOB}(-\delta, \delta) = \int_{-\delta}^{\delta} dx p_M(x|c_0, \dots, c_k). \quad (78)$$

For a fixed DOB, one can thus give the corresponding uncertainty interval $\pm\delta$. In what follows, we consider $\text{DOB} = 0.68$. We note that the interval $\pm\delta$ would correspond to the usual 1σ uncertainty for Gaussian distributions $p_M(\Delta|c_0, \dots, c_k)$. Our probability distributions (65) and (70) are, however, not Gaussians.

B. Uncertainty quantification for energy levels

Uncertainty quantification is a two-step procedure. First we adjust LECs to data. Second, we quantify uncertainties based on assumptions about the distributions of LECs.

At LO, the energy spectrum is that of a harmonic quadrupole oscillator [see Eq. (16)], and the LEC ω has to be adjusted to data. For nuclear vibrations in the mass $A \approx 100$ region, $\omega \approx 0.6$ MeV. Thus, the distribution of this LEC is relatively sharp. It is neither log-normal distributed nor without a scale (i.e., log-uniform distributed). In what follows, we fix the LEC ω for each nucleus by performing a least-square fit of the objective function

$$\chi_{\text{LO}}^2 = \sum_s \frac{[E_{\text{exp}}(s) - E_{\text{LO}}(s)]^2}{\sigma_{\text{exp}}^2 + \sigma_{\text{LO}}^2}. \quad (79)$$

Here the sum is over states $s = 2_1^+, 0_2^+, 2_2^+$, and 4_1^+ . In the fit, the theoretical uncertainty is estimated as

$$\sigma_{\text{LO}} = \omega \left[\frac{E_{\text{LO}}(s)}{\Lambda} \right]^2, \quad (80)$$

and the experimental uncertainty is neglected because $\sigma_{\text{exp}} \ll \sigma_{\text{LO}}$.

At NLO, three new LECs (g_N , g_v , and g_I) enter the determination of the energies; see Eq. (38). Instead of readjusting ω at NLO, we replace it with $\omega \rightarrow \omega + g_\omega$, keep the value of ω at what was obtained at LO, and adjust g_ω . Thus, we rewrite

$$E_{\text{NLO}} = \omega N + g_\omega N + g_N N^2 + g_v v(v+3) + g_I I(I+1). \quad (81)$$

It is clear that the parameters g_N , g_v , g_I , and g_ω are expected to scale as ω^3/Λ^2 . In an EFT, one assumes that $g_\alpha \Lambda^2/\omega^3$ (for $\alpha = N, v, I, \omega$) are of order unity and constrained by log-normal distributions. We adjust these coefficients to data by

minimizing the objective function

$$\chi_{\text{NLO}}^2 = \sum_s \frac{[E_{\text{exp}}(s) - E_{\text{NLO}}(s)]^2}{\sigma_{\text{exp}}^2 + \sigma_{\text{NLO}}^2}. \quad (82)$$

Here the employed states s are as for the LO fit, but the theoretical uncertainty is estimated as

$$\sigma_{\text{NLO}} = \omega \left[\frac{E_{\text{LO}}(s)}{\Lambda} \right]^3. \quad (83)$$

Again, the experimental uncertainty is neglected because $\sigma_{\text{exp}} \ll \sigma_{\text{NLO}}$. As we adjust four parameters to four data points, the fit is exact.

Let us now turn to the quantification of theoretical uncertainties. We note that simple uncertainty estimates can be based on the naive estimates (80) and (83) at LO and NLO, respectively. For quantified uncertainties we adapt the methods of the previous section to the problem at hand.

We start with uncertainty quantification at LO. As discussed above, the distribution for ω is a Dirac δ function, and LO uncertainties are attributed solely to assumptions about the distribution of LECs from higher orders. Thus,

$$p_1^{(\text{hw})}(\Delta) = \frac{e^{\frac{\sigma^2}{2}}}{4\varepsilon^2} \left[1 - \Phi \left(\frac{\sigma}{\sqrt{2}} \left[1 + \frac{\log(\Delta/\varepsilon^2)}{\sigma^2} \right] \right) \right] \quad (84)$$

for the hard-wall prior (58), and

$$p_M^{(\text{G})}(\Delta) = \frac{1}{2\pi\sigma qs} \int_0^\infty dx e^{-\frac{\log^2 x}{2\sigma^2}} e^{-\frac{\Delta^2 x^2}{2q^2 s^2}} \quad (85)$$

for the Gaussian prior (59). Here $q^2 \equiv \sum_{m=k+1}^{k+M} \varepsilon^{2m}$, with $k=0$ for uncertainties owing to M terms above the LO contribution. In Eq. (84) it is assumed that the uncertainty comes fully from the term proportional to ε^2 .

We now turn to uncertainty quantification at NLO. Returning to Eq. (81), the NLO energy correction for the state $|N, v, I\rangle$ is $\omega\varepsilon^2 c_2$, with

$$\begin{aligned} c_2 &\equiv c_2(N, v, I) \\ &= \frac{g_\omega N + g_N N^2 + g_v v(v+3) + g_I I(I+1)}{\varepsilon^2 \omega}. \end{aligned} \quad (86)$$

Table I shows the resulting coefficients c_2 for each state of the nuclei ^{62}Ni , $^{98,100}\text{Ru}$, $^{106,108}\text{Pd}$, $^{110,112,114}\text{Cd}$, and $^{118,120,122}\text{Te}$ considered in this work. These nuclei exhibit low-energy spectra that resemble a harmonic quadrupole oscillator. All coefficients c_2 are of order one. Thus, the products $\omega\varepsilon c_2$ are of natural size. Also shown are the values of the vibrational scale ω for each nucleus and the LEC Q_0 associated with the quadrupole moment; see Sec. III. We note that these quadrupole moments are an order of magnitude smaller than for rotational nuclei [3].

To determine a valid prior for the coefficients c_2 we turn to the distribution of the coefficients c_2 for an ensemble consisting of one-phonon and two-phonon states in the nuclei we study. The cumulative distribution is shown in Fig. 1. It is well approximated by a Gaussian prior (59) with parameter $s \approx 0.65$, or by a hard-wall prior (58), once the mean is shifted from zero to $\bar{c}_2 \approx 1$. We note that the cumulative distribution is practically unchanged when c_2 values from three-phonon

TABLE I. Values for the vibrational energy ω (in keV), the coefficients c_2 in states up to the two-phonon level, and the LEC Q_0^2 associated with the quadrupole moment (in Weisskopf units) for the nuclei studied in this work.

Nucleus	ω (keV)	$c_2(2_1^+)$	$c_2(0_2^+)$	$c_2(2_2^+)$	$c_2(4_1^+)$	Q_0^2 (W.U.)
^{62}Ni	1147.9	0.55	-0.29	0.19	0.26	10.6
^{98}Ru	668.1	1.02	0.57	0.88	0.83	27.8
^{100}Ru	573.9	2.35	1.39	2.36	1.79	23.6
^{106}Pd	541.8	1.80	1.38	1.36	1.80	30.4
^{108}Pd	464.5	1.14	1.53	0.90	1.51	36.9
^{110}Cd	696.7	1.57	1.32	1.33	1.56	21.1
^{112}Cd	635.2	1.72	0.82	1.14	1.52	23.2
^{114}Cd	578.3	1.72	0.93	1.23	1.53	21.8
^{118}Te	582.9	0.83	-0.52	0.19	0.40	-
^{120}Te	567.8	0.79	0.32	0.71	0.56	31.0
^{122}Te	593.5	-0.08	0.88	0.48	0.17	40.7

states are included in the analysis. We employ $\sigma = \log(3/2)$ in the log-normal prior (57).

Finally, we turn to uncertainty quantification at NLO for individual nuclei. For the hard-wall prior we find

$$p_1^{(\text{hw})}(\Delta|c_2) = \frac{e^{\frac{3\sigma^2}{2}}}{2\varepsilon^3} \frac{1 - \Phi\left(\frac{\sigma}{\sqrt{2}}\left[2 + \frac{\log(\kappa)}{\sigma^2}\right]\right)}{1 - \Phi\left(\frac{\sigma}{\sqrt{2}}\left[1 + \frac{\log(|c_2'|)}{\sigma^2}\right]\right)}. \quad (87)$$

Here $\kappa \equiv \max(|c_2'|, \Delta/\varepsilon^3)$ and $c_2' \equiv c_2 - \bar{c}_2$. For the Gaussian prior we find

$$p_M^{(\text{G})}(\Delta|c_2) = \frac{\int_0^\infty dx x e^{-\frac{\log^2 x}{2\sigma^2}} e^{-\frac{(c_2^2 + \Delta^2/q^2)x^2}{2s^2}}}{\sqrt{2\pi} qs \int_0^\infty dx e^{-\frac{\log^2 x}{2\sigma^2}} e^{-\frac{c_2^2 x^2}{2s^2}}}. \quad (88)$$

In the determination of the prior, we employed an ensemble of nuclei. To assess the consistency of this approach and to verify the statistical interpretation of the quantified uncertainties, we compare EFT predictions for the one-phonon and

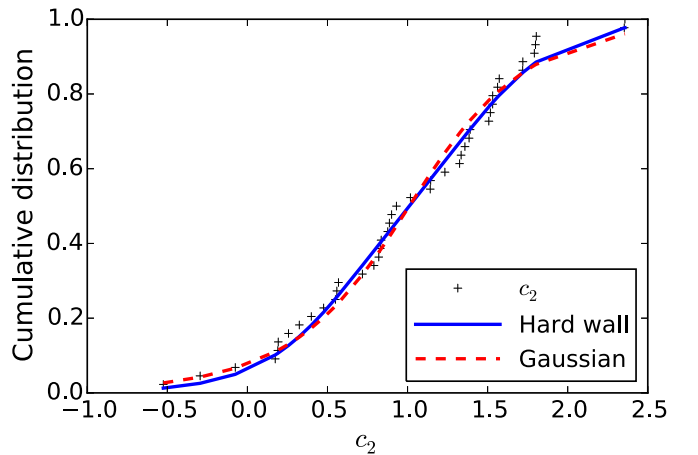


FIG. 1. (Color online) Cumulative distribution for the c_2 coefficients for states up to the two-phonon level in the ensemble of all nuclei studied in this work. The cumulative distributions of the hard-wall and Gaussian priors are also shown for comparison.

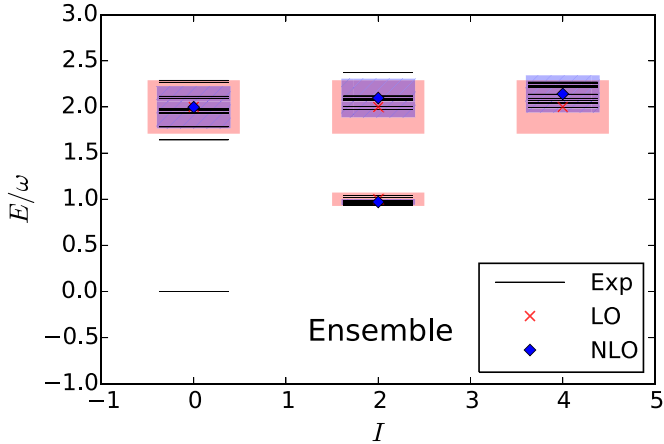


FIG. 2. (Color online) Comparison between the normalized energies E/ω of the one- and two-phonon states as a function of spin I in the ensemble of the nuclei studied in this work. Experimental energies are shown as thick black lines. LO and NLO energies are shown as red crosses and blue diamonds, respectively. Theoretical uncertainties quantified from 68% DOB intervals are shown as shaded and hatched areas at LO and NLO, respectively.

two-phonon states of these nuclei. To do so, we first normalize the energies by dividing them by the nucleus-dependent ω and then perform χ^2 fits at LO and NLO. The results are shown in Fig. 2. Experimental data, LO calculations, and NLO calculations are shown as black lines, red crosses, and blue diamonds, respectively. The theoretical uncertainty at each order, displayed as a shaded area of the corresponding color, are 68% DOB intervals obtained with the Gaussian prior. We note that 82% of the 44 one- and two-phonon states lie within the NLO theoretical uncertainty. This is within 1σ ($1/\sqrt{44} \approx 15\%$) of the expected 68% for the ensemble size. Thus, the statistical interpretation of our DOB intervals is consistent for the energies.

C. Uncertainty quantification for quadrupole moments

We quantify uncertainties for LO transition quadrupole moments as follows. The expansion for these matrix elements is

$$\langle f || Q || i \rangle = \langle f || Q || i \rangle_{\text{LO}} \left(1 + \sum_{i=1} c_i \varepsilon^i \right), \quad (89)$$

and coefficients c_i are expected to be of order one. The expansion for the $B(E2)$ transition strength (51) is obtained from the expansion (89) of the corresponding matrix element. We quantify uncertainties for these matrix elements and transition strengths based on Eq. (85) with $s = 1$ and compute 68% DOB intervals.

To summarize this section, we have derived analytical formulas for uncertainty quantification based on log-normal priors. For uncertainty quantification of LO results for energies and matrix elements we employ Eq. (85) with $s = 0.65$ and $s = 1$, respectively, and compute 68% DOB intervals. For uncertainty quantification at NLO for energies, we confirmed that the prior for the employed expansion coefficients is based on data from an ensemble of vibrational nuclei. Based on this ensemble, Eqs. (87) and (88) describe the distribution of

uncertainties. These are then used for the computation of 68% DOB intervals.

IV. ENERGY SPECTRA WITH QUANTIFIED UNCERTAINTIES

To test the EFT, we compare the low-energy spectra and reduced transition probabilities of the nuclei ^{62}Ni , $^{98,100}\text{Ru}$, $^{106,108}\text{Pd}$, $^{110,112,114}\text{Cd}$, and $^{118,120,122}\text{Te}$ against LO and NLO results. We consider nuclei in which the ratio of energies $E(4_1^+)/E(2_1^+) \approx 2$, states with the spins of the two-phonon triplet are at about $2E(2_1^+)$, and states with the spins of the three-phonon quintuplet are around $3E(2_1^+)$. First, we discuss the description of the energy spectra by the EFT. The LECs required for such description were obtained from χ^2 fits at LO and NLO, with a breakdown scale set to $\Lambda = 3\omega$, based on the appearance of states that cannot be identified with harmonic quadrupole excitations.

The low-lying spectrum of ^{62}Ni exhibits states with the spins and energies of a harmonic quadrupole vibrator up to the three-phonon level, making this nucleus a candidate for low-energy vibrational behavior. The breakdown of vibrational motion at the three-phonon level agrees with the results and discussion for this nucleus presented in Ref. [15], where shell-model calculations with a ^{40}Ca core were required to simultaneously describe the energies and electromagnetic properties of some multiphonon candidates. Similar results for this and other nickel isotopes [55,56] suggest that intruder configurations need to be taken into account in a microscopic description of spectra and electromagnetic properties of the low-lying states in these nuclei.

Figure 3 shows the comparison between experimental data taken from Ref. [57], LO and NLO calculations for energies up to the three-phonon level for this nucleus. States up to the two-phonon level are shown as thick black lines, while states above them are shown as thin lines only if their spins have been

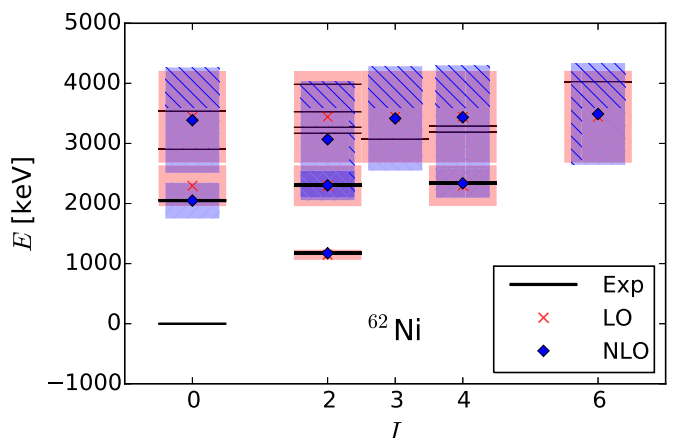


FIG. 3. (Color online) Partial energy spectrum of ^{62}Ni up to the three-phonon level. Experimental data [57], shown as black lines, are compared to LO and NLO calculations, shown as red crosses and blue diamonds, respectively. States up to the two-phonon level are shown as thick black lines. Theoretical uncertainties quantified from 68% DOB intervals are shown as shaded and hatched areas at LO and NLO, respectively.

assigned (consequently, some of the nuclei studied in this work exhibit a higher density of states above the two-phonon level than displayed in the figures). The uncertainty at each order is shown as 68% DOB areas. The increased level density above the two-phonon states is consistent with our identification of the breakdown scale at about the three-phonon level. Below the breakdown level, the description of the experimental data is improved order by order. We note that the LO and NLO predictions for three-phonon energies are relatively close.

Let us make three more comments that apply to ^{62}Ni and the other nuclei studied in what follows. First, LO predictions are consistent with data within the quantified theoretical uncertainties. Second, we note that the energies up to the two-phonon states are accurately described at NLO, because the EFT Hamiltonian exhibits four adjustable LECs. Thus, EFT predictions are accurate (they agree with data) yet not very precise (theoretical uncertainties are considerable). The comparison of LO and NLO results shows the convergence properties of the EFT. Third, we also note that the prediction for the $I = 6$ three-phonon state is quite accurate. It thus seems that the breakdown scale for yrast states could be higher than for the other states. This is presumably attributable to the lower level density of high-spin states.

Figure 4 compares the energy spectrum of ^{98}Ru and ^{100}Ru and our calculations. Again, the breakdown scale seems properly identified. We note that the differences between LO and NLO predictions for three-phonon levels are considerable.

The ruthenium isotopes near the $N = 50$ shell closure appear to undergo a transition from spherical to triaxial shapes, based on the behavior of the ratio $R_{4/2} \equiv E(4_1^+)/E(2_1^+)$ with increasing neutron number [60]. From this chain, ^{98}Ru is the first isotope expected to exhibit collective behavior based on its ratio of energies $R_{4/2} \approx 2$. Its low-energy spectrum exhibits vibrational-like excitations, with several nonvibrational states above the two-phonon level. Experimental energies were taken from Ref [58]. For ^{100}Ru , experimental data were taken from Ref. [59]. Shell-model calculations with neutrons promoted across the $N = 50$ shell gap reveal the importance of single-particle motion in these isotopic chain [61,62]. As mentioned before, ruthenium isotopes transit from spherical to triaxial shapes as the neutron number increases. Larger deviations from the harmonic behavior in ^{100}Ru suggest that its shape is farther away from sphericity than that of ^{98}Ru .

The energy spectra of ^{106}Pd and ^{108}Pd are compared against LO and NLO calculations in Fig. 5. In ^{108}Pd there are fewer levels around the three-phonon states. The considerable deviations of the $I = 0, 2$ three-phonon energies from NLO predictions—consistent with the theoretical uncertainties—nevertheless suggests that the breakdown scale has been identified correctly.

The energy spectra and enhanced transitions probabilities for decays from the low-lying states in palladium isotopes, assumed to be spherical, suggest vibrational motion in these systems. For ^{106}Pd and ^{108}Pd , experimental data were taken from Ref. [63] and Ref. [64], respectively. Single-particle states have been suggested for ^{108}Pd [65]. The palladium isotopes exhibit ratios $R_{4/2} \approx 2.4$ and $B(E2; 4_1^+ \downarrow)/B(E2; 2_1^+ \downarrow) \approx 1.6$. These quantities, in addition to the large diagonal quadrupole matrix elements for states up to the two-phonon level in palladium

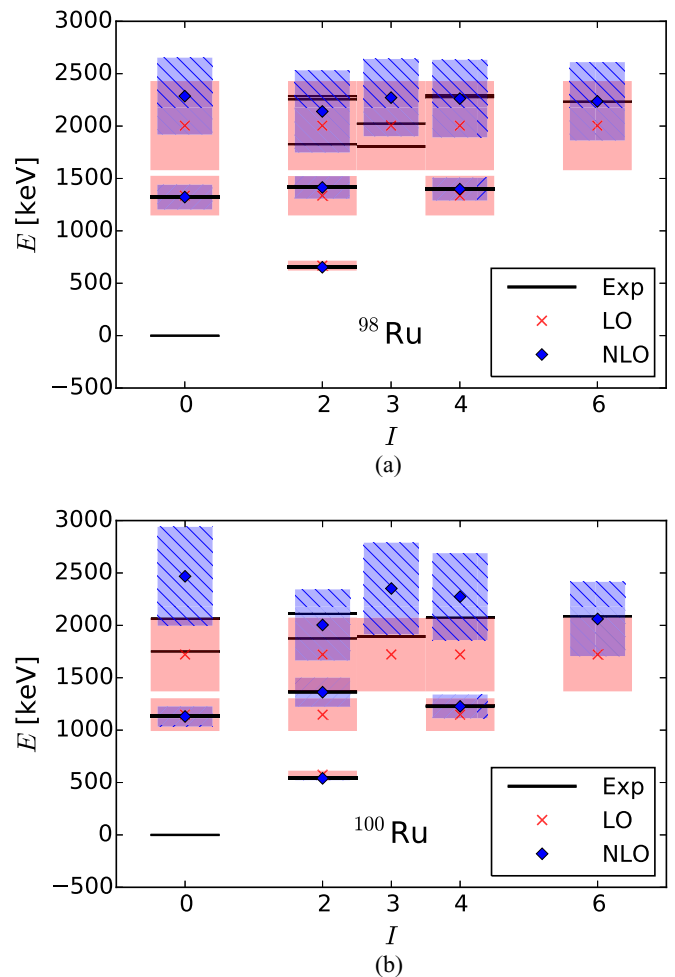


FIG. 4. (Color online) Partial energy spectrum of ^{98}Ru (a) and ^{100}Ru (b) up to the three-phonon level. Experimental data [58,59], shown as black lines, are compared to LO and NLO calculations, shown as red crosses and blue diamonds, respectively. States up to the two-phonon level are shown as thick black lines. Theoretical uncertainties quantified from 68% DOB intervals are shown as shaded and hatched areas at LO and NLO, respectively.

isotopes [66], strongly suggest that the deviation from the harmonic oscillator behavior in these systems is considerable.

Figure 6 compares experimental spectra of cadmium isotopes with LO and NLO results from the EFT. We note that the deviations from expectations for the harmonic quadrupole vibrator are pronounced in these isotopes, with additional energy levels just above the two-phonon states. We also note that the energies of the three-phonon 6_1^+ states deviate more strongly from EFT predictions than the other nuclei we consider in this work. In these nuclei, the breakdown scale for vibrations is clearly low. From the EFT's perspective anharmonic corrections are expected to be most significant.

The cadmium isotopes have once been considered textbook candidates of low-energy vibrational behavior based only on their energy spectra [3–5], despite exhibiting intruder states owing to protons promoted across the $Z = 50$ shell gap around the two-phonon level [70,71]. Other studies on cadmium isotopes [7,8,11,13,20,22] in which mixing between

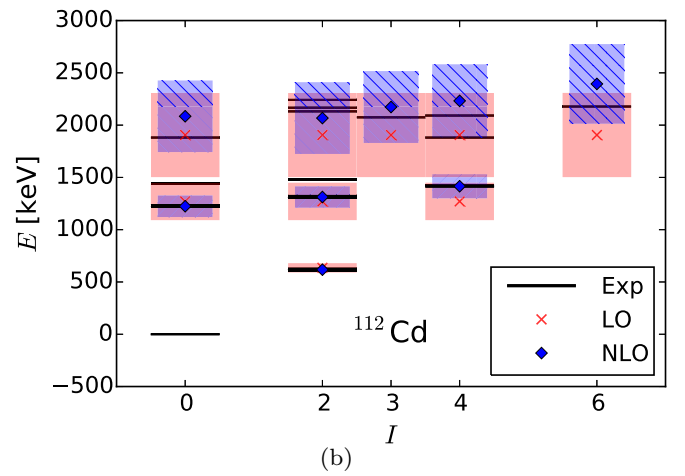
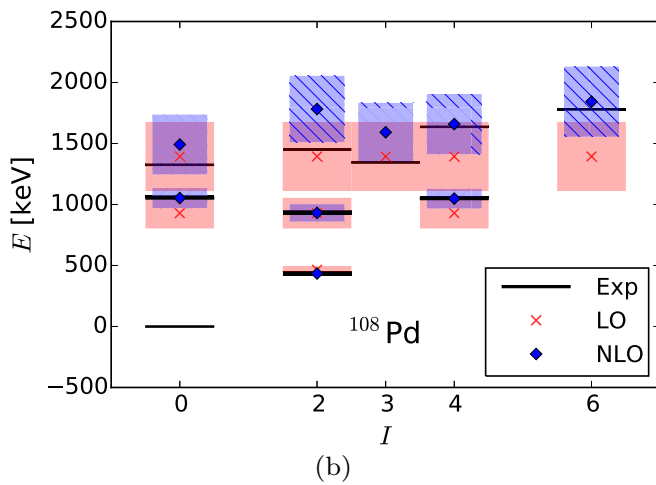
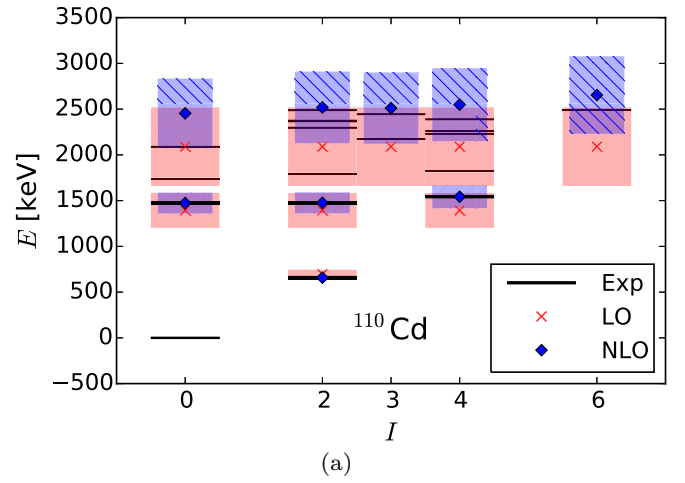
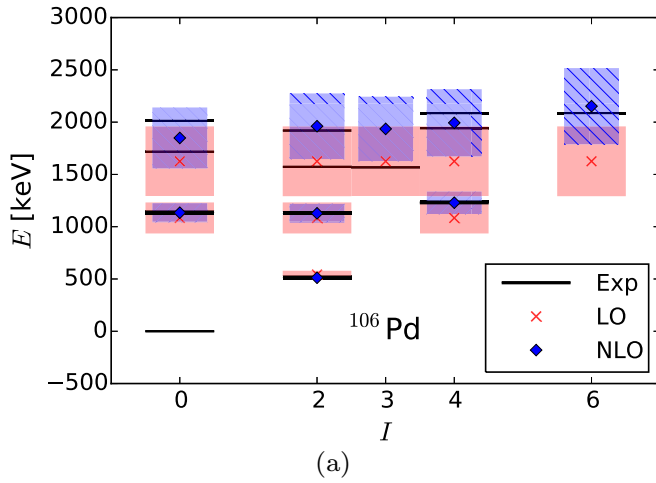


FIG. 5. (Color online) Partial energy spectrum of ^{106}Pd (a) and ^{108}Pd (b) up to the three-phonon level. Experimental data [63,64], shown as black lines, are compared to LO and NLO calculations, shown as red crosses and blue diamonds, respectively. States up to the two-phonon level are shown as thick black lines. Theoretical uncertainties quantified from 68% DOB intervals are shown as shaded and hatched areas at LO and NLO, respectively.

vibrational and nonvibrational states is taken into account, cannot accurately describe the electromagnetic properties of multiphonon candidates. They set the breakdown of vibrational behavior at the two- or three-phonon level depending on the isotope, and suggest a quasirotational character for the low-lying excitations, based on the large quadrupole moments of some yrast states [20,72]. For the three isotopes studied in this work, $A = 110, 112, 114$, experimental data were taken from Refs. [67–69], respectively. The 0_2^+ and 2_2^+ states were employed as the two-phonon states for the χ^2 fits. The states identified as members of two-phonon triplet in this work might be in disagreement with previous studies [11,13,20], where, for example, the 0_2^+ in ^{112}Cd have been identified as an intruder state [70,73]. Here the identification is made based on the assumption that nonvibrational modes require more energy to be excited. As we discuss in Sec. V, $B(E2)$ values for decays

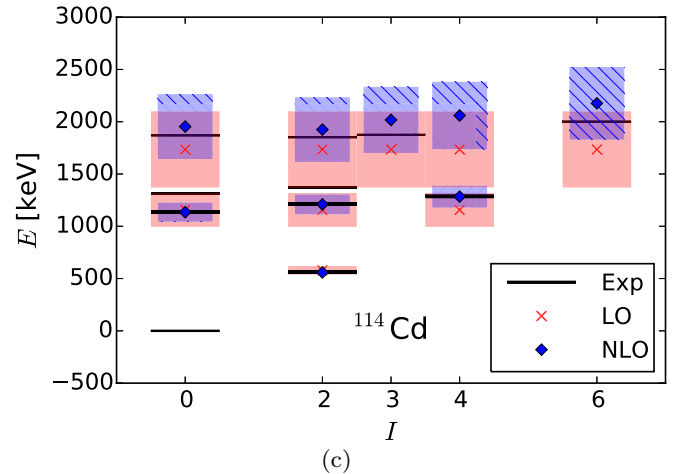


FIG. 6. (Color online) Partial energy spectrum of ^{110}Cd (a), ^{112}Cd (b), and ^{114}Cd (c) up to the three-phonon level. Experimental data [67–69], shown as black lines, are compared to LO and NLO calculations, shown as red crosses and blue diamonds, respectively. States up to the two-phonon level are shown as thick black lines. Theoretical uncertainties quantified from 68% DOB intervals are shown as shaded and hatched areas at LO and NLO, respectively.

from the identified states seems to be in better agreement with the EFT expectations than those from other states.

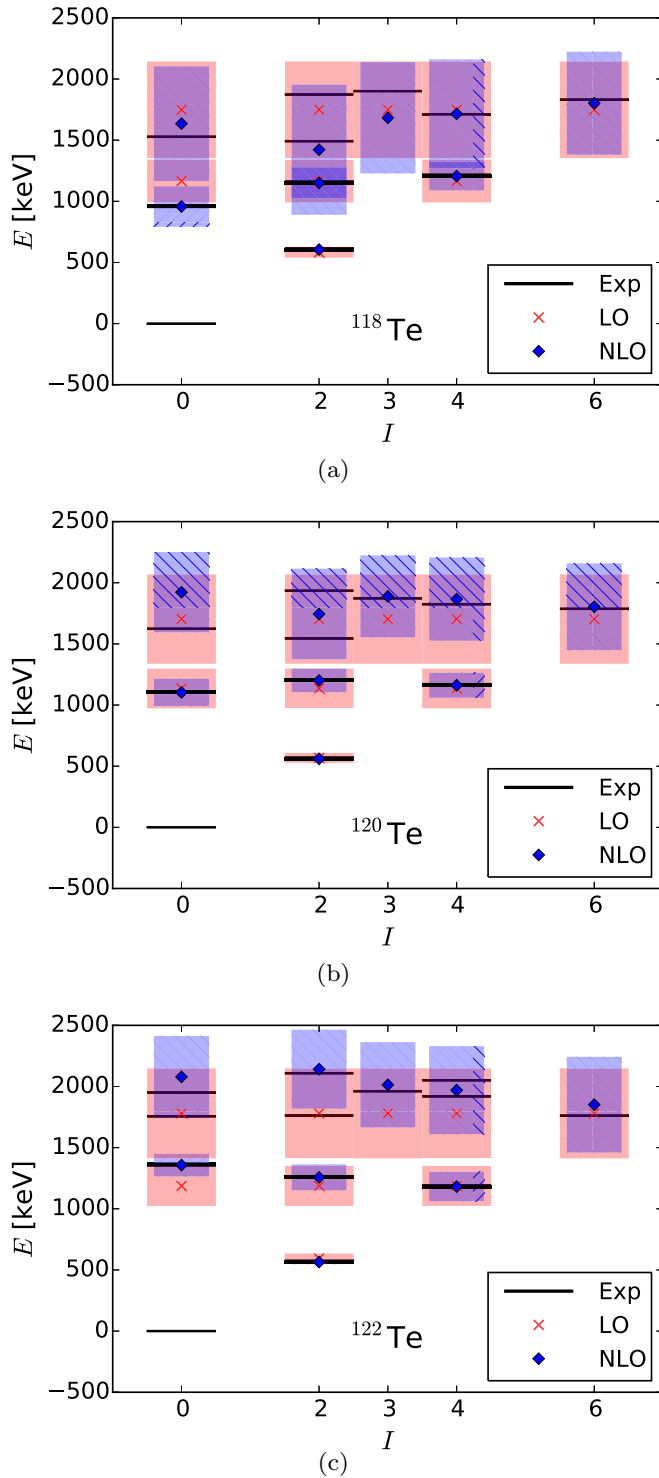


FIG. 7. (Color online) Partial energy spectrum of ^{118}Te (a), ^{120}Te (b), and ^{122}Te (c) up to the three-phonon level. Experimental data [74–76], shown as black lines, are compared to LO and NLO calculations, shown as red crosses and blue diamonds, respectively. States up to the two-phonon level are shown as thick black lines. Theoretical uncertainties quantified from 68% DOB intervals are shown as shaded and hatched areas at LO and NLO, respectively.

Figure 7 shows the comparison between experimental data taken from Refs. [74–76] for ^{118}Te , ^{120}Te , and ^{122}Te ,

respectively, LO and NLO results from EFT. The tellurium isotopic chain provides us with candidates of low-energy vibrational behavior. The isotopes with $A = 118, 120, 122$ all exhibit very similar spectra with states that can be identified with those of a quadrupole vibrator up to the three-phonon level. From these isotopes, the best candidate is ^{120}Te with a nonvibrational state slightly above the three-phonon quintuplet. ^{118}Te and ^{122}Te exhibit a nonvibrational state already at the three-phonon level. The breakdown of the collective behavior is a consequence of competing single-particle motion, known to exist in tellurium isotopes [77–82], and signaled in ^{122}Te by the unusual energy ratios $E(4_1^+)/E(2_1^+) < 2$ and $E(6_1^+)/E(4_1^+) < 1.5$ [83]. The alignment of both valence nucleons and protons promoted across the $Z = 50$ shell gap breaks the spherical symmetry and gives rise to noncollective deformed states. These states compete energetically with the collective states. In particular, the 6_1^+ state has been interpreted both as a vibrational state or in terms of valence protons coupled to a tin core.

Let us summarize our uncertainties as 68% DOB intervals $\pm\delta$ for the hard-wall (hw) prior and the Gaussian (G) prior. The uncertainty is $\omega\delta$ for the energy levels. At LO, the pdfs in Eqs. (84) and (85) agree with each other and yield values of $\delta = 0.07$ and $\delta = 0.29$ for the one- and two-phonon levels, respectively. Table II summarizes the values of δ for states up to the two-phonon level at NLO. The columns labeled by hw and G show the values of δ obtained from the pdfs in Eqs. (87) and (88), respectively. With the exception of a few relatively large uncertainties, both priors yield very similar results. For large uncertainties δ , one samples the tails of the respective priors, and these are notably different (and not well constrained by data; cf. Fig. 1).

V. ELECTROMAGNETIC MOMENTS: COMPARISON WITH DATA

In this section, we compare our results for transition quadrupole moments, diagonal quadrupole matrix elements,

TABLE II. Values of the uncertainties at NLO, with $\pm\delta$ giving the size of 68% DOB intervals in states up to the two-phonon level. The uncertainty arising from the hard-wall (hw) and Gaussian (G) priors are calculated as 68% DOB intervals of the distribution functions (87) and (88), respectively.

Nucleus	2_1^+		0_2^+		2_2^+		4_1^+	
	hw	G	hw	G	hw	G	hw	G
^{62}Ni	0.02	0.02	0.29	0.22	0.21	0.20	0.20	0.20
^{98}Ru	0.02	0.02	0.18	0.19	0.18	0.18	0.18	0.18
^{100}Ru	0.04	0.03	0.18	0.18	0.30	0.22	0.21	0.20
^{106}Pd	0.03	0.02	0.18	0.18	0.18	0.18	0.21	0.20
^{108}Pd	0.02	0.02	0.18	0.19	0.18	0.18	0.18	0.19
^{110}Cd	0.02	0.02	0.18	0.18	0.18	0.18	0.19	0.19
^{112}Cd	0.02	0.02	0.18	0.18	0.18	0.18	0.18	0.19
^{114}Cd	0.02	0.02	0.18	0.18	0.18	0.18	0.18	0.19
^{118}Te	0.02	0.02	0.34	0.23	0.21	0.20	0.19	0.19
^{120}Te	0.02	0.02	0.19	0.19	0.18	0.18	0.18	0.19
^{122}Te	0.03	0.03	0.18	0.18	0.18	0.19	0.21	0.20

and magnetic moments with data. Theoretical uncertainties are quantified for all quadrupole observables we consider. As we will see, the EFT correctly captures and consistently describes the main experimental features of vibrational nuclei.

To determine the LEC Q_0 , we perform χ^2 fits to data at LO with

$$\chi_{\text{LO}}^2 = \sum_t \frac{[B(E2)_{\text{exp}}^{(t)} - B(E2)_{\text{LO}}^{(t)}]^2}{\sigma_{\text{exp}}^2 + \sigma_{\text{LO}}^2}. \quad (90)$$

Here t labels the transitions from the one-phonon state to the ground state and from the two-phonon states to the one-phonon state, i.e., $2_1^+ \rightarrow 0_1^+$, $0_2^+ \rightarrow 2_1^+$, $2_2^+ \rightarrow 2_1^+$, and $4_1^+ \rightarrow 2_1^+$. In these fits we estimate the theoretical uncertainty for decays from the N -phonon state as

$$\sigma_{\text{LO}} = B(E2)_{\text{LO}}^{(t)} \varepsilon. \quad (91)$$

Experimental data were taken mostly from the Nuclear Data Sheets for the studied nuclei. For ^{62}Ni , these data were complemented with those from Ref. [15], while for ^{98}Ru we took the data from Ref. [16], which establish a ratio $B(E2, 4_1^+ \rightarrow 2_1^+)/B(E2, 2_1^+ \rightarrow 0_1^+) = 1.86(16)$ in agreement with the expectations for vibrators instead of taking data for which this ratio has anomalous values [10,60,61]. The lack of experimental data for ^{118}Te makes it impossible to perform a χ^2 fit. For ^{120}Te , we fixed Q_0^2 to the only experimental value and make predictions for decays from the two-phonon states.

Table III compares experimental and theoretical $B(E2)$ values (in Weisskopf units) for each nucleus considered in this work. The theoretical uncertainty is shown as 68% DOB intervals from the pdf (85) with $s = 1$. Within the often considerable theoretical uncertainties, the EFT consistently describes the available experimental data. These results, taken together with the results for energy level in Table II, show that vibrational nuclei can be described as such within an EFT with a breakdown scale around the three-phonon level. They are examples for anharmonic quadrupole oscillators.

How reasonable and consistent are the 68% DOB intervals for the $B(E2)$ transitions? To address this question, we turn

TABLE III. $B(E2)$ values (in Weisskopf units) for decays from states below the three-phonon level in the ensemble of all studied nuclei. Experimental data are in agreement with LO calculations within theoretical uncertainty, given by the 68% DOB interval for the normalized residual for $B(E2)$ values.

Nucleus	$2_1^+ \rightarrow 0_1^+$	EFT	$0_2^+ \rightarrow 2_1^+$	$2_2^+ \rightarrow 2_1^+$	$4_1^+ \rightarrow 2_1^+$	EFT
^{62}Ni	12.1(4)	11(4)	42(23)	14.9(42)	21(6)	21(7)
^{98}Ru	31(1)	28(9)		47(5)	57.6(40)	56(19)
^{100}Ru	35.6(4)	24(8)	35(5)	30.9(4)	51(4)	47(16)
^{106}Pd	44.3(15)	30(10)	35(8)	44(4)	76(11)	61(20)
^{108}Pd	49.5(13)	37(12)	52(5)	71(5)	73(8)	74(25)
^{110}Cd	27.0(8)	21(7)		30(5)	42(9)	42(14)
^{112}Cd	30.2(3)	23(8)	51(14)	15(3)	61(6)	46(15)
^{114}Cd	31.1(19)	22(7)	27.4(17)	22(6)	62(4)	43(15)
^{120}Te	31(6)	31(10)				62(21)
^{122}Te	36.9(3)	41(14)		100(30)		81(27)

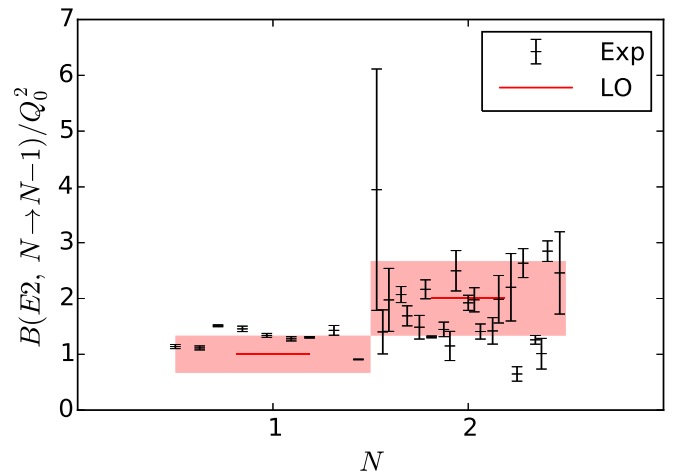


FIG. 8. (Color online) Comparison between the normalized $B(E2)$ values for decays from the one- and two-phonon states in the ensemble of the nuclei studied in this work. Experimental $B(E2)$ values are shown as black lines with error bars. Theoretical uncertainties quantified from 68% DOB intervals are shown as shaded areas.

again to the ensemble of vibrational nuclei considered in this work. Excluding the isotopes $^{118,120}\text{Te}$, the EFT prediction $B(E2)/Q_0^2 = N$ for decays from the N -phonon state can be compared to the data from all nuclei in the ensemble. This comparison is shown in Fig. 8, where the experimental data and the LO calculations are shown as black error bars and red lines with shaded uncertainty bands, respectively. About 81% of the data are within the 68% DOB intervals. This is a consistent agreement for an ensemble of 32 data points.

The eigenstates of a harmonic quadrupole oscillator have vanishing diagonal quadrupole matrix elements. Compared to this ideal case, diagonal quadrupole matrix elements for isotopes of Cd and Pd exhibit sizes that are only somewhat smaller than transition quadrupole moments. From the EFT's perspective, sizable diagonal quadrupole matrix elements are expected. Comparing the expansion of the spectrum (38) with that of the quadrupole operator (44) shows that anharmonic corrections have relative size ε for energies and relative size $\varepsilon^{1/2}$ for the quadrupole operator.

Let us consider diagonal quadrupole matrix elements (49). We employ experimental data for the diagonal quadrupole matrix elements of the 2_1^+ , 2_2^+ , and 4_1^+ in ^{106}Pd and ^{108}Pd from Svensson *et al.* and determine the LEC Q_1 by a χ^2 fit to these data. In these fits, the theoretical uncertainty was estimated as $Q_0 \varepsilon^{3/2}$ as discussed in Sec. II C.

The fits yield $Q_1 = -0.14$ eb for both palladium isotopes. (We recall that for a nucleus with A nucleons 1 W.U. = $5.94 \times 10^{-6} A^{4/3} e^2 b^2$.) Comparing the size of Q_1 against Q_0 yields $Q_1/Q_0 = 0.47$ and $Q_1/Q_0 = 0.41$ in ^{106}Pd and ^{108}Pd , respectively. These ratios are consistent with the EFT estimate $Q_1/Q_0 \sim \varepsilon^{1/2} = \sqrt{1/3} \approx 0.58$. In other words, sizable diagonal quadrupole matrix elements are not a surprise for these anharmonic vibrators but rather expected and attributable to the marginal separation of scales, i.e., the breakdown of the EFT around the three-phonon level.

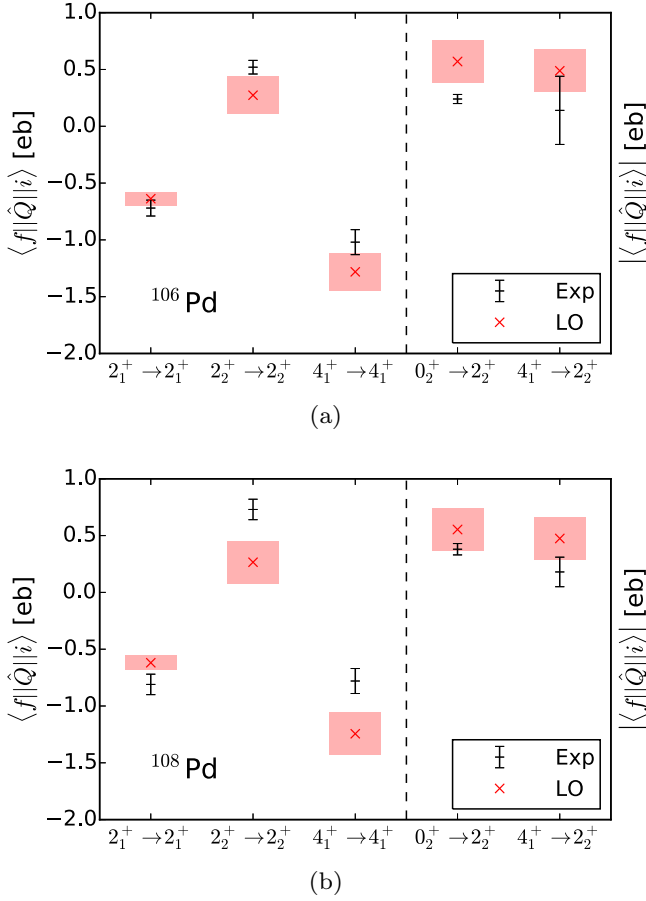


FIG. 9. (Color online) Reduced electric quadrupole matrix elements in ^{106}Pd (a) and ^{108}Pd (b). Experimental data, shown as black lines with error bars, are compared LO calculations, shown as red crosses. Theoretical uncertainties from 68% DOB intervals are shown as shaded areas. The left side shows diagonal matrix elements employed in the fit of the LEC constant Q_1 . The right side shows predictions for the absolute values of the reduced matrix elements governing $E2$ transitions between two-phonon states.

The left part of both panels in Fig. 9 compares EFT results to data [66] for the diagonal quadrupole matrix elements of the 2_1^+ , 2_2^+ , and 4_1^+ states in ^{106}Pd and ^{108}Pd . Theoretical uncertainties are shown as 68% DOB bands. They are based on the Gaussian prior (59) and $M = 1$ in Eq. (65). Within the theoretical uncertainties, the EFT is consistent with the data.

We turn to transition quadrupole moments (48) between two-phonon states because these are also determined by the LEC Q_1 and are thus predictions of the EFT. The right part of Fig. 9 shows the magnitude of the transition matrix elements and compares them to data [66]. We note that the EFT yields different signs of these (nonobservable) matrix elements and that only the magnitude of these matrix elements is an observable quantity; see the definition of the observable $B(E2)$ transition strength in Eq. (51).

Theoretical results for quadrupole matrix elements in ^{114}Cd are shown in Fig. 10 and compared to data [84]. The uncertainties are quantified as for the palladium isotopes. With the exception of the diagonal matrix element of the 2_2^+ state,

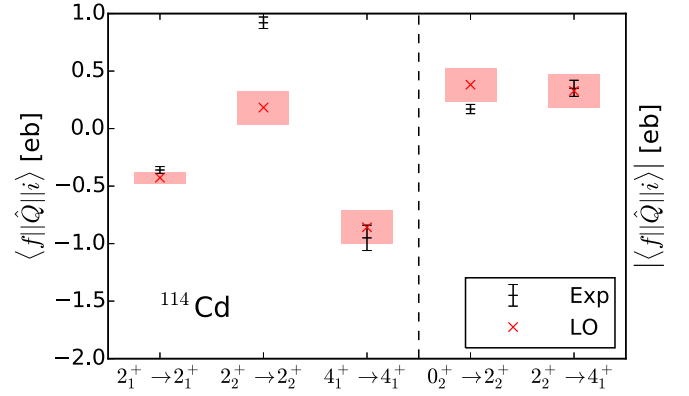


FIG. 10. (Color online) Comparison between data and EFT results for some reduced quadrupole matrix elements in ^{114}Cd . Experimental data, shown as black lines with error bars, are compared LO calculations, shown as red crosses. Theoretical uncertainties from 68% DOB intervals are shown as shaded areas. The left side shows diagonal matrix elements employed in the fit of the LEC constant Q_1 . The right side shows predictions for the absolute values of the reduced matrix elements governing $E2$ transitions between two-phonon states.

the EFT yields a consistent description of the data and has predictive power for the off-diagonal matrix elements. Here $Q_0 = 0.27$ e.b., and $Q_1 = -0.09$ e.b.

Thus, the EFT consistently describes matrix elements of electromagnetic operators. In the present approach, the anharmonicities are attributable to the operators themselves, with states being the eigenstates of the harmonic quadrupole oscillator. We note that Figs. 9 and 10 exhibit very similar patterns for the different nuclei. As a last consistency check, we turn to magnetic moments.

The EFT needs one magnetic moment to determine a LEC, i.e., the constant g in Eq. (53). While magnetic moments are typically known for the lowest 2^+ state in many even-even nuclei [72], the EFT can only be tested if more magnetic moments are known below the three-phonon level. The states 2_1^+ , 2_2^+ , and 4_1^+ have nonzero spins and thus exhibit magnetic moments. As discussed below Eq. (53), the EFT predicts at LO that both 2^+ states have equal magnetic moments, i.e., $\mu(2_1^+) = \mu(2_2^+) \equiv \mu(2^+)$, and that the 4^+ state has a magnetic moment $\mu(4_1^+) = \sqrt{6}\mu(2^+) \approx 2.44\mu(2^+)$. Weighted averages of the experimental data [72] [in units of nuclear magnetons (nm)] for ^{106}Pd show that $\mu(2_1^+) \approx 0.79 \pm 0.02$ nm, $\mu(2_2^+) = 0.71 \pm 0.10$ nm, and $\mu(4_1^+) = 1.8 \pm 0.4$ nm. This is consistent with EFT expectations. It would certainly be interesting to test these EFT predictions in other vibrational nuclei.

Overall, the EFTs results and predictions for electromagnetic properties of states and transitions below the three-phonon level are consistent with data. This would make it interesting to measure such complete data sets for other vibrational nuclei as well.

VI. SUMMARY

We developed an EFT for collective nuclear vibrations based on quadrupole degrees of freedom, rotational invariance, and a breakdown scale at around the three-phonon level. For

spectra, the EFT is driven to next-to-leading order, while the computation of other matrix elements is restricted to LO. The terms appearing in the Hamiltonian and quadrupole operator differ from those employed in several models.

The EFT approach also allows us to quantify theoretical uncertainties. To this purpose, we make testable assumptions about priors regarding the distribution of LECs and employ recently developed tools from Bayesian statistics. We give analytical results for the important case of log-normal priors. The priors employed in the uncertainty quantification of energies are consistent for the ensemble of nuclei we considered.

The EFT is minimally coupled to electromagnetic gauge fields in a model-independent way, with nonminimal couplings accounting for subleading corrections. For states below the three-phonon level we describe LO $B(E2)$ transition strengths with quantified uncertainties and present several results for diagonal and off-diagonal matrix elements of the quadrupole operator. Comparing the EFT results to an extensive data set shows that spectra and transition strengths are consistently described within the theoretical and experimental uncertainties for ^{62}Ni , $^{98,100}\text{Ru}$, $^{106,108}\text{Pd}$, $^{110,112,114}\text{Cd}$, and $^{118,120,122}\text{Te}$. In particular, relatively large diagonal matrix elements in

$^{106,108}\text{Pd}$ and ^{114}Cd are consistent with the expectations of the EFT. The consistent description of spectra, $E2$ transitions and matrix elements, and magnetic moments within the EFT for nuclear vibration suggests that the nuclei studied in this work can be viewed as anharmonic quadrupole vibrators. This work also suggests that it would be interesting to measure a combination of matrix elements for electric and magnetic observables in nuclei such as ^{120}Te and ^{122}Te .

It would be interesting to extend the EFT of nuclear vibrations also to odd-mass neighbors of the even-even nuclei considered in this work. Combining, for instance, halo EFT with this work, one might explore to what extent such nuclei can be understood by coupling the odd nucleon to the quadrupole degrees of freedom of vibrational even-even nuclei.

ACKNOWLEDGMENTS

This material is based upon work supported by the U.S. Department of Energy, Office of Science, Office of Nuclear Physics under Grant No. DEFG02-96ER40963 (University of Tennessee) and under Contract No. DE-AC05-00OR22725 (Oak Ridge National Laboratory).

APPENDIX: ANALYTICAL RESULTS FOR LOG-NORMAL PRIORS

In this appendix we present some details for the derivation of analytical results for the combination of log-normal priors (57) and hw priors (58).

The denominator of Eq. (60) is

$$\int_0^\infty dc \text{pr}(c) \prod_{m=0}^k \text{pr}^{(\text{hw})}(c_m|c) = \frac{2^{-(k+1)}}{\sqrt{2\pi}\sigma} \int_a^\infty dc c^{-(k+2)} e^{-\frac{1}{2\sigma^2}(\log c)^2}. \quad (\text{A1})$$

Here

$$a \equiv \max(|c_0|, \dots, |c_k|) \quad (\text{A2})$$

is a function of the expansion coefficients. Substitutions $z = \log c$ and $x = z - \log(a)$ yield

$$\frac{e^{-(k+1)\log a} e^{-\frac{1}{2\sigma^2}(\log a)^2}}{2^{(k+1)}\sqrt{2\pi}\sigma} \int_0^\infty dx e^{-\frac{x^2}{2\sigma^2} - x(k+1 + \frac{\log a}{\sigma^2})}. \quad (\text{A3})$$

This integral is known [54], and we find

$$2^{-(k+2)} e^{\frac{\sigma^2}{2}(k+1)^2} \left[1 - \Phi\left(\frac{\sigma}{\sqrt{2}}\left(k+1 + \frac{\log a}{\sigma^2}\right)\right) \right] \quad (\text{A4})$$

as the final result for the denominator of Eq. (60). Here $\Phi(x) \equiv (2/\sqrt{\pi}) \int_0^x dt \exp(-t^2)$ denotes the error function. The numerator of the expression (60) can be evaluated in similar fashion. Employing the shorthand

$$b \equiv \max\left(a, \frac{|\Delta|}{\varepsilon^{k+1}}\right) \quad (\text{A5})$$

we find for the numerator of Eq. (60)

$$\frac{e^{\frac{\sigma^2}{2}(k+2)^2}}{2^{k+3}\varepsilon^{k+1}} \left[1 - \Phi\left(\frac{\sigma}{\sqrt{2}}\left(k+2 + \frac{\log b}{\sigma^2}\right)\right) \right]. \quad (\text{A6})$$

Thus, for $M = 1$,

$$p_1^{(\text{hw})}(\Delta|c_0, \dots, c_k) = \frac{e^{\frac{2k+3}{2}\sigma^2} \left[1 - \Phi\left(\frac{\sigma}{\sqrt{2}}\left(k+2 + \frac{\log b}{\sigma^2}\right)\right) \right]}{2\varepsilon^{k+1} \left[1 - \Phi\left(\frac{\sigma}{\sqrt{2}}\left(k+1 + \frac{\log a}{\sigma^2}\right)\right) \right]}, \quad (\text{A7})$$

and the dependence on the expansion coefficients is entirely contained in the functions a and b .

Let us continue and compute $p_2^{(\text{hw})}(\Delta|c)$. The integral (68) is again known for $M = 2$ [54], and the final result is

$$p_2^{(\text{hw})}(\Delta|c) = \begin{cases} \frac{1}{2\varepsilon^{k+1}c}, & |\Delta| \leq (1-\varepsilon)\varepsilon^{k+1}c, \\ 0, & |\Delta| > (1+\varepsilon)\varepsilon^{k+1}c, \\ \frac{(1+\varepsilon)\varepsilon^{k+1}c-|\Delta|}{4\varepsilon^{2k+3}c^2}, & \text{else.} \end{cases} \quad (\text{A8})$$

As we need to integrate over c for the computation of $p_2^{(\text{hw})}(\Delta|C_0, \dots, C_k)$, we rewrite this function as

$$p_2^{(\text{hw})}(\Delta|c) = \begin{cases} 0 & \text{for } c \leq \frac{|\Delta|}{(1+\varepsilon)\varepsilon^{k+1}}, \\ \frac{1}{2\varepsilon^{k+1}c} & \text{for } c > \frac{|\Delta|}{(1-\varepsilon)\varepsilon^{k+1}}, \\ \frac{(1+\varepsilon)\varepsilon^{k+1}c-|\Delta|}{4\varepsilon^{2k+3}c^2} & \text{else.} \end{cases} \quad (\text{A9})$$

The remaining integrations are similar to the ones solved above, and one finds

$$p_2^{(\text{hw})}(\Delta|c_0, \dots, c_k) = \frac{(2\varepsilon^{k+1})^{-1} e^{\frac{2k+3}{2}\sigma^2}}{1 - \Phi\left(\frac{\sigma}{\sqrt{2}}\left(k+1 + \frac{\log a}{\sigma^2}\right)\right)} \left\{ 1 - \Phi\left(\frac{\sigma}{\sqrt{2}}\left(k+2 + \frac{\log d}{\sigma^2}\right)\right) \right. \\ \left. + \frac{1+\varepsilon}{2\varepsilon} \Theta(g-f) \left[\Phi\left(\frac{\sigma}{\sqrt{2}}\left(k+2 + \frac{\log g}{\sigma^2}\right)\right) - \Phi\left(\frac{\sigma}{\sqrt{2}}\left(k+2 + \frac{\log f}{\sigma^2}\right)\right) \right] \right. \\ \left. - \frac{|\Delta|}{2\varepsilon^{k+2}} \Theta(g-f) e^{\frac{2k+5}{2}\sigma^2} \left[\Phi\left(\frac{\sigma}{\sqrt{2}}\left(k+3 + \frac{\log g}{\sigma^2}\right)\right) - \Phi\left(\frac{\sigma}{\sqrt{2}}\left(k+3 + \frac{\log f}{\sigma^2}\right)\right) \right] \right\}. \quad (\text{A10})$$

Here Θ denotes the unit step function, and the expressions

$$d \equiv \max\left(a, \frac{|\Delta|}{(1-\varepsilon)\varepsilon^{k+1}}\right), \quad (\text{A11})$$

$$f \equiv \max\left(a, \frac{|\Delta|}{(1+\varepsilon)\varepsilon^{k+1}}\right), \quad (\text{A12})$$

$$g \equiv \frac{|\Delta|}{(1-\varepsilon)\varepsilon^{k+1}}, \quad (\text{A13})$$

encode much of the functional dependence.

For $M > 2$, the evaluation of $p_M^{(\text{hw})}(\Delta|c)$ [Eq. (68)] becomes increasingly tedious. Fortunately, $p_2^{(\text{hw})}(\Delta|c)$ is a good approximation even for $M > 2$. The quality of this approximation can be verified by inserting the expression (68) into Eq. (60) and performing the integrations numerically. We note that the accuracy of the $M = 2$ result is not surprising. As the expansion coefficients c_n are natural in size, increasingly higher orders contribute little to the residual (56). This makes Eq. (A10) the main result of this appendix.

-
- [1] A. Bohr, The coupling of nuclear surface oscillations to the motion of individual nucleons, *Dan. Mat. Fys. Medd.* **26**, 14 (1952).
- [2] A. Bohr and B. R. Mottelson, Collective and individual-particle aspects of nuclear structure, *Dan. Mat. Fys. Medd.* **27**, 16 (1953).
- [3] A. Bohr and B. R. Mottelson, *Nuclear Structure: Nuclear Deformation* (W. A. Benjamin, Reading, MA, 1975), Vol. II.
- [4] J. Kern, P. Garrett, J. Jolie, and H. Lehmann, Search for nuclei exhibiting the U(5) dynamical symmetry, *Nucl. Phys. A* **593**, 21 (1995).
- [5] D. J. Rowe and J. L. Wood, *Fundamentals of Nuclear Models: Foundational Models* (World Scientific, Singapore, 2010), Vol. I.
- [6] H. Lehmann, P. E. Garrett, J. Jolie, C. A. McGrath, M. Yeh, and S. W. Yates, On the nature of “three-phonon” excitations in ^{112}Cd , *Phys. Lett. B* **387**, 259 (1996).
- [7] F. Corminboeuf, T. B. Brown, L. Genilloud, C. D. Hannant, J. Jolie, J. Kern, N. Warr, and S. W. Yates, Characterization of Three-Phonon States in ^{110}Cd , *Phys. Rev. Lett.* **84**, 4060 (2000).
- [8] M. Kadi, N. Warr, P. E. Garrett, J. Jolie, and S. W. Yates, Vibrational and intruder structures in ^{116}Cd , *Phys. Rev. C* **68**, 031306 (2003).
- [9] S. W. Yates, Probing multiphonon excitations in nearly spherical nuclei with fast neutrons, *J. Phys. G: Nucl. Part. Phys.* **31**, S1393 (2005).
- [10] E. Williams, C. Plettner, E. A. McCutchan, H. Levine, N. V. Zamfir, R. B. Cakirli, R. F. Casten, H. Ai, C. W. Beausang, G. Gurdal, A. Heinz, J. Qian, D. A. Meyer, N. Pietralla, and V. Werner, Revisiting anomalous $B(E2; 4_1^+ \rightarrow 2_1^+)/B(E2; 2_1^+ \rightarrow 0_1^+)$ values in ^{98}Ru and ^{180}Pt , *Phys. Rev. C* **74**, 024302 (2006).
- [11] P. E. Garrett, K. L. Green, H. Lehmann, J. Jolie, C. A. McGrath, M. Yeh, and S. W. Yates, Properties of ^{112}Cd from the $(n, n' \gamma)$ reaction: Lifetimes and transition rates, *Phys. Rev. C* **75**, 054310 (2007).
- [12] D. Bandyopadhyay, S. R. Leshner, C. Fransen, N. Boukharouba, P. E. Garrett, K. L. Green, M. T. McEllistrem, and S. W. Yates, Investigation of phonon excitations in ^{114}Cd with the $(n, n' \gamma)$ reaction, *Phys. Rev. C* **76**, 054308 (2007).

- [13] P. E. Garrett, K. L. Green, and J. L. Wood, Breakdown of vibrational motion in the isotopes $^{110-116}\text{Cd}$, *Phys. Rev. C* **78**, 044307 (2008).
- [14] J. C. Batchelder *et al.*, Collective and noncollective states in ^{116}Cd studied via the β decays of $^{116}\text{Ag}^{m1,m2,gs}$, *Phys. Rev. C* **80**, 054318 (2009).
- [15] A. Chakraborty, J. N. Orce, S. F. Ashley, B. A. Brown, B. P. Crider, E. Elhami, M. T. McEllistrem, S. Mukhopadhyay, E. E. Peters, B. Singh, and S. W. Yates, Status of vibrational structure in ^{62}Ni , *Phys. Rev. C* **83**, 034316 (2011).
- [16] D. Radeck, V. Werner, G. Ilie, N. Cooper, V. Anagnostatou, T. Ahn, L. Bettermann, R. J. Casperson, R. Chevrier, A. Heinz, J. Jolie, D. McCarthy, M. K. Smith, and E. Williams, Simultaneous deorientation and lifetime measurement in ^{98}Ru using the recoil distance Doppler shift method in inverse Coulomb excitation, *Phys. Rev. C* **85**, 014301 (2012).
- [17] J. C. Batchelder, N. T. Brewer, R. E. Goans, R. Grzywacz, B. O. Griffith, C. Jost, A. Korgul, S. H. Liu, S. V. Paulauskas, E. H. Spejewski, and D. W. Stracener, Low-lying collective states in ^{120}Cd populated by β decay of ^{120}Ag : Breakdown of the anharmonic vibrator model at the three-phonon level, *Phys. Rev. C* **86**, 064311 (2012).
- [18] J. de Boer, R. G. Stokstad, G. D. Symons, and A. Winther, Reorientation Effect in Cd^{114} , *Phys. Rev. Lett.* **14**, 564 (1965).
- [19] D. R. Bès and G. G. Dussel, Phenomenological treatment of anharmonic effects in Cd isotopes, *Nucl. Phys. A* **135**, 1 (1969).
- [20] P. E. Garrett and J. L. Wood, On the robustness of surface vibrational modes: case studies in the Cd region, *J. Phys. G: Nucl. Part. Phys.* **37**, 069701 (2010).
- [21] S. W. Yates, On quadrupole vibrations in nearly spherical nuclei, *J. Phys.: Conf. Ser.* **381**, 012048 (2012).
- [22] P. E. Garrett *et al.*, Detailed spectroscopy of ^{110}Cd : Evidence for weak mixing and the emergence of γ -soft behavior, *Phys. Rev. C* **86**, 044304 (2012).
- [23] U. V. Kolck, Effective field theory of nuclear forces, *Prog. Part. Nucl. Phys.* **43**, 337 (1999).
- [24] P. F. Bedaque and U. van Kolck, Effective field theory for few-nucleon systems, *Annu. Rev. Nucl. Part. Sci.* **52**, 339 (2002).
- [25] E. Epelbaum, H.-W. Hammer, and U.-G. Meißner, Modern theory of nuclear forces, *Rev. Mod. Phys.* **81**, 1773 (2009).
- [26] R. Machleidt and D. Entem, Chiral effective field theory and nuclear forces, *Phys. Rept.* **503**, 1 (2011).
- [27] P. Navrátil, S. Quaglioni, I. Stetcu, and B. R. Barrett, Recent developments in no-core shell-model calculations, *J. Phys. G: Nucl. Part. Phys.* **36**, 083101 (2009).
- [28] B. R. Barrett, P. Navrátil, and J. P. Vary, Ab initio no core shell model, *Prog. Part. Nucl. Phys.* **69**, 131 (2013).
- [29] G. Hagen, T. Papenbrock, M. Hjorth-Jensen, and D. J. Dean, Coupled-cluster computations of atomic nuclei, *Rep. Prog. Phys.* **77**, 096302 (2014).
- [30] C. Bertulani, H.-W. Hammer, and U. van Kolck, Effective field theory for halo nuclei: shallow p-wave states, *Nucl. Phys. A* **712**, 37 (2002).
- [31] R. Higa, H.-W. Hammer, and U. van Kolck, $\alpha\alpha$ scattering in halo effective field theory, *Nucl. Phys. A* **809**, 171 (2008).
- [32] H.-W. Hammer and D. Phillips, Electric properties of the Beryllium-11 system in Halo EFT, *Nucl. Phys. A* **865**, 17 (2011).
- [33] E. Ryberg, C. Forssén, H.-W. Hammer, and L. Platter, Effective field theory for proton halo nuclei, *Phys. Rev. C* **89**, 014325 (2014).
- [34] T. Papenbrock, Effective theory for deformed nuclei, *Nucl. Phys. A* **852**, 36 (2011).
- [35] E. A. Coello Pérez and T. Papenbrock, Effective theory for the nonrigid rotor in an electromagnetic field: Toward accurate and precise calculations of $E2$ transitions in deformed nuclei, *Phys. Rev. C* **92**, 014323 (2015).
- [36] T. Papenbrock and H. A. Weidenmüller, Effective field theory for finite systems with spontaneously broken symmetry, *Phys. Rev. C* **89**, 014334 (2014).
- [37] T. Papenbrock and H. A. Weidenmüller, Effective field theory of emergent symmetry breaking in deformed atomic nuclei, *J. Phys. G: Nucl. Part. Phys.* **42**, 105103 (2015).
- [38] M. Schindler and D. Phillips, Bayesian methods for parameter estimation in effective field theories, *Ann. Phys.* **324**, 682 (2009).
- [39] M. Cacciari and N. Houdeau, Meaningful characterisation of perturbative theoretical uncertainties, *J. High Energy Phys.* **09** (2011) 039.
- [40] E. Bagnaschi, M. Cacciari, A. Guffanti, and L. Jenniches, An extensive survey of the estimation of uncertainties from missing higher orders in perturbative calculations, *J. High Energy Phys.* **02** (2015) 133.
- [41] R. J. Furnstahl, D. R. Phillips, and S. Wesolowski, A recipe for EFT uncertainty quantification in nuclear physics, *J. Phys. G: Nucl. Part. Phys.* **42**, 034028 (2015).
- [42] R. J. Furnstahl, N. Klco, D. R. Phillips, and S. Wesolowski, Quantifying truncation errors in effective field theory, *Phys. Rev. C* **92**, 024005 (2015).
- [43] D. J. Dean and M. Hjorth-Jensen, Pairing in nuclear systems: from neutron stars to finite nuclei, *Rev. Mod. Phys.* **75**, 607 (2003).
- [44] D. A. Varshalovich, A. N. Moskalev, and V. K. Khersonskii, *Quantum Theory of Angular Momentum* (World Scientific, Singapore, 1988).
- [45] F. Iachello and A. Arima, *The Interacting Boson Model* (Cambridge University Press, Cambridge, U.K., 1987).
- [46] M. A. Caprio, D. J. Rowe, and T. A. Welsh, Construction of $\text{SO}(5)\supset\text{SO}(3)$ spherical harmonics and Clebsch–Gordan coefficients, *Comput. Phys. Commun.* **180**, 1150 (2009).
- [47] G. Gneuss, U. Mosel, and W. Greiner, A new treatment of the collective nuclear hamiltonian, *Phys. Lett. B* **30**, 397 (1969).
- [48] G. Gneuss and W. Greiner, Collective potential energy surfaces and nuclear structure, *Nucl. Phys. A* **171**, 449 (1971).
- [49] P. O. Hess, M. Seiwert, J. Maruhn, and W. Greiner, General collective model and its application to $^{238}_{92}\text{U}$, *Z. Phys. A: At. Nucl.* **296**, 147 (1980).
- [50] P. O. Hess, J. Maruhn, and W. Greiner, The general collective model applied to the chains of Pt, Os and W isotopes, *J. Phys. G: Nucl. Phys.* **7**, 737 (1981).
- [51] J. M. Eisenberg and W. Greiner, *Nuclear Theory: Excitation Mechanisms of the Nucleus* (North-Holland, Amsterdam, 1970).
- [52] D. G. Ireland and W. Nazarewicz, Enhancing the interaction between nuclear experiment and theory through information and statistics, Uncertainty analysis and order-by-order optimization of chiral nuclear interactions, *J. Phys. G: Nucl. Part. Phys.* **42**, 030301 (2015).
- [53] B. D. Carlsson, A. Ekström, C. Forssén, D. Fahlin Strömberg, G. R. Jansen, O. Lilja, M. Lindby, B. A. Mattsson, and K. A. Wendt, [arXiv:1506.02466](https://arxiv.org/abs/1506.02466) [nucl-th].
- [54] I. S. Gradshteyn and I. M. Ryzhik, *Table of Integrals, Series, and Products* 8th ed., edited by D. Zwillinger and V. Moll (Academic Press, Waltham, MA, 2014).
- [55] O. Kenn, K.-H. Speidel, R. Ernst, J. Gerber, P. Maier-Komor, and F. Nowacki, Measurements of g factors and lifetimes of low

- lying states in $^{58-64}\text{Ni}$ and their shell model implications, *Phys. Rev. C* **63**, 064306 (2001).
- [56] J. N. Orce, B. Crider, S. Mukhopadhyay, E. Peters, E. Elhami, M. Scheck, B. Singh, M. T. McEllistrem, and S. W. Yates, Determination of the $2_1^+ \rightarrow 0_1^+$ transition strengths in ^{58}Ni and ^{60}Ni , *Phys. Rev. C* **77**, 064301 (2008).
- [57] A. L. Nichols, B. Singh, and J. K. Tuli, Nuclear data sheets for $A = 62$, *Nucl. Data Sheets* **113**, 973 (2012).
- [58] B. Singh and Z. Hu, Nuclear data sheets for $A = 98$, *Nucl. Data Sheets* **98**, 335 (2003).
- [59] B. Singh, Nuclear data sheets for $A = 100$, *Nucl. Data Sheets* **109**, 297 (2008).
- [60] R. B. Cakirli, R. F. Casten, E. A. McCutchan, H. Ai, H. Amro, M. Babilon, C. W. Beausang, A. Heinz, R. O. Hughes, D. A. Meyer, C. Plettner, J. J. Ressler, and N. V. Zamfir, Breakdown of vibrational structure in ^{98}Ru , *Phys. Rev. C* **70**, 044312 (2004).
- [61] B. Kharraja, U. Garg, S. S. Ghugre, H. Jin, R. V. F. Janssens, I. Ahmad, H. Amro, M. P. Carpenter, S. Fischer, T. L. Khoo, T. Lauritsen, D. Nisius, W. Reviol, W. F. Mueller, L. L. Riedinger, R. Kaczarowski, E. Ruchowska, W. C. Ma, and I. M. Govil, Recoil-distance lifetime measurements in $^{96,97,98}\text{Ru}$: Search for possible onset of collectivity at $N \sim 52$, *Phys. Rev. C* **61**, 024301 (1999).
- [62] J. Timár, J. Gizon, A. Gizon, D. Sohler, B. M. Nyakó, L. Zolnai, A. J. Boston, D. T. Joss, E. S. Paul, A. T. Semple, C. M. Parry, and I. Ragnarsson, Terminating bands in $^{98,99,100}\text{Ru}$ nuclei: New information on the neutron $2d_{5/2}$ and $1g_{7/2}$ energy spacing, *Phys. Rev. C* **62**, 044317 (2000).
- [63] D. D. Frenne and A. Negret, Nuclear data sheets for $A = 106$, *Nucl. Data Sheets* **109**, 943 (2008).
- [64] J. Blachot, Nuclear data sheets for $A = 108$, *Nucl. Data Sheets* **91**, 135 (2000).
- [65] P. H. Regan, T. M. Menezes, C. J. Pearson, W. Gelletly, C. S. Purry, P. M. Walker, S. Juutinen, R. Julin, K. Helariutta, A. Savelius, P. Jones, P. Jämsen, M. Muikku, P. A. Butler, G. Jones, and P. Greenlees, Observation of $(h_{11/2})^2$ neutron alignments in ^{100}Mo , ^{104}Ru , and ^{108}Pd using deep inelastic reactions, *Phys. Rev. C* **55**, 2305 (1997).
- [66] L. E. Svensson, C. Fahlander, L. Hasselgren, A. Bäcklin, L. Westerberg, D. Cline, T. Czosnyka, C. Y. Wu, R. M. Diamond, and H. Kluge, Multiphonon vibrational states in $^{106,108}\text{Pd}$, *Nucl. Phys. A* **584**, 547 (1995).
- [67] G. Gurdal and F. Kondev, Nuclear data sheets for $A = 110$, *Nucl. Data Sheets* **113**, 1315 (2012).
- [68] D. Frenne and E. Jacobs, Nuclear data sheets for $A = 112$, *Nucl. Data Sheets* **79**, 639 (1996).
- [69] J. Blachot, Nuclear data sheets for $A = 114$, *Nucl. Data Sheets* **113**, 515 (2012).
- [70] K. Heyde, P. Van Isacker, M. Waroquier, G. Wenes, and M. Sambataro, Description of the low-lying levels in $^{112,114}\text{Cd}$, *Phys. Rev. C* **25**, 3160 (1982).
- [71] R. A. Meyer and L. Peker, Evidence for the coexistence of shapes in even-mass Cd nuclei, *Z. Phys. A: At. Nucl.* **283**, 379 (1977).
- [72] N. Stone, Table of nuclear magnetic dipole and electric quadrupole moments, *At. Data Nucl. Data Tables* **90**, 75 (2005).
- [73] J. Wood, K. Heyde, W. Nazarewicz, M. Huyse, and P. van Duppen, Coexistence in even-mass nuclei, *Phys. Rep.* **215**, 101 (1992).
- [74] K. Kitao, Nuclear data sheets update for $A = 118$, *Nucl. Data Sheets* **75**, 99 (1995).
- [75] K. Kitao, Y. Tendow, and A. Hashizume, Nuclear data sheets for $A = 120$, *Nucl. Data Sheets* **96**, 241 (2002).
- [76] T. Tamura, Nuclear data sheets for $A = 122$, *Nucl. Data Sheets* **108**, 455 (2007).
- [77] E. S. Paul, D. B. Fossan, J. M. Sears, and I. Thorslund, Favored noncollective oblate states in light tellurium isotopes, *Phys. Rev. C* **52**, 2984 (1995).
- [78] E. S. Paul, D. B. Fossan, G. J. Lane, J. M. Sears, I. Thorslund, and P. Vaska, High-spin states in $^{121,122}\text{Te}$: Identification of favored noncollective oblate states, *Phys. Rev. C* **53**, 1562 (1996).
- [79] J. R. Vanhoy, R. T. Coleman, K. A. Crandell, S. F. Hicks, B. A. Sklaney, M. M. Walbran, N. V. Warr, J. Jolie, F. Corminboeuf, L. Genilloud, J. Kern, J.-L. Schenker, and P. E. Garrett, Structure of ^{120}Te from the $^{118}\text{Sn}(\alpha, 2n\gamma)$ reaction and ^{120}I decay, *Phys. Rev. C* **68**, 034315 (2003).
- [80] S. F. Hicks, G. K. Alexander, C. A. Aubin, M. C. Burns, C. J. Collard, M. M. Walbran, J. R. Vanhoy, E. Jensen, P. E. Garrett, M. Kadi, A. Martin, N. Warr, and S. W. Yates, Intruder structures observed in ^{122}Te through inelastic neutron scattering, *Phys. Rev. C* **71**, 034307 (2005).
- [81] S. F. Hicks, J. R. Vanhoy, and S. W. Yates, Fragmentation of mixed-symmetry excitations in stable even-even tellurium nuclei, *Phys. Rev. C* **78**, 054320 (2008).
- [82] S. Nag *et al.*, Collective and noncollective states in ^{120}Te , *Phys. Rev. C* **85**, 014310 (2012).
- [83] J. A. Cizewski, Energy ratios in medium and heavy mass nuclei. Signatures of coexisting configurations, *Phys. Lett. B* **219**, 189 (1989).
- [84] C. Fahlander, A. Bäcklin, L. Hasselgren, A. Kavka, V. Mittal, L. E. Svensson, B. Varnevig, D. Cline, B. Kotlinski, H. Grein, E. Grosse, R. Kulesa, C. Michel, W. Spreng, H. J. Wollersheim, and J. Stachel, Quadrupole collective properties of ^{114}Cd , *Nucl. Phys. A* **485**, 327 (1988).